(5 units/mL), streptomycin (100 μg/mL), penicillin (100 units/mL), and fungizone (0.25 μg/mL). The PBMCs were placed in two-well chambers coated with 0.2% gelatin (17, 18) and incubated at 37°C in a humidified environment with a 5% CO_2 atmosphere. Monocytes and mature endothelial colonies attached to the well chambers within 3 days. The nonadherent cells were transferred to other wells in EGM after 3 days. After 2 weeks, the endothelial colonies were characterized by the metabolic uptake of acetylated low-density lipoprotein labeled with 1,1′-dioctadecyl-3,3,3′,3′-tetramethylindocarbocyanine perchlorate (DiI-Ac-LDL; Biomedical Technologies, Stoughton, MA). The cells were incubated with 10 μg/mL DiI-Ac-LDL at 37°C for 4 hours and examined by fluorescence microscopy. DiI-Ac-LDL and GFP double-positive colonies that formed at 2 weeks were considered late-outgrowth colonies (17).

Measurement of local blood perfusion in superficial tumor tissue. The blood perfusion of the tumors was measured using a laser Doppler perfusion imaging (LDPI) system (Moor Instruments, Devon, United Kingdom; refs. 35, 36). The LDPI data were acquired from mice on day 10 following five antibody treatments given at 24-hour intervals. Each mouse was anesthetized 15 minutes before the recordings to eliminate artifacts caused by body movements; the mouse was placed on a heating plate at 40°C, and the LDPI recording was made (35, 36).

Estimation of vascular endothelial growth factor levels in subcutaneuse tumors and cultured supernatants. The tumor tissues were harvested on day 14 after five antibody treatments and homogenized with a tissue homogenizer in 9 volumes of lysis buffer [300 mmol/L NaCl, 15 mmol/L Tris-HCl, 2 mmol/L $MgCl_2$, 2 mmol/L Triton X-100, 20 ng/mL pepstatin A, 20 ng/mL leupeptin, 20 ng/mL aprotinin (pH 7.4)]. A total of 3×10^5 Colon38 or PancO2 cells were seeded in six-well plates and incubated with fetal bovine serum–free medium containing 10 μg/mL normal IgG or 10 μg/mL anti-CXCR4-neutralizing antibody for 24 hours. The ELISA assay for VEGF was done by the SRL analysis service (Tokyo, Japan).

Statistical analysis. The data are expressed as mean ± SE. Comparisons between the groups were analyzed using Student's t test. $P < 0.05$ was considered statistically significant.

Results

CXCR4-positive cells contribute to the establishment of tumor tissues in a cancer cell type–independent manner. To estimate the role of the SDF-1/CXCR4 axis in the establishment of gastrointestinal tumors, in addition to its known metastasis-promoting ability, we analyzed two models of s.c. tumors in mice using two mouse-derived cancer cells, Colon38 and PancO2. CXCR4 mRNA was not detected in cultured PancO2 cells but was detected in Colon38 cells (Fig. 1*A*). However, CXCR4-positive cells were detected in the tissues of tumors established from implanted Colon38 and PancO2 cells; the CXCR4-positive cells were observed around the tumor vessels and occasionally in the endothelium (Fig. 1*B, arrow*). These findings suggested that the cells infiltrating the tumor might express CXCR4 regardless of whether the cancerous cells themselves express CXCR4. To clearly distinguish cancer cells from TICs, we established a mouse model in which the bone marrow was depleted by irradiation and then reconstituted by transplantation of GFP-tagged bone marrow cells (GFP-BMT mice). Many bone marrow–derived cells were found to infiltrate into both types of tumor tissues, and GFP and CXCR4 double-positive cells were detected around the tumor vessels (Fig. 1*C, arrow*). To confirm the expression of CXCR4 in the TICs, TICs were isolated from tumor tissues as described previously, and the expression levels of various chemokine receptors were analyzed by RT-PCR (data not shown). CXCR4 mRNA was detected in the TICs of both Colon38 and PancO2 tumors (Fig. 1*A*). To investigate the percentage of CXCR4-expressing cells in bone marrow–derived cells, we counted the total numbers of GFP and CXCR4 double-positive cells as the

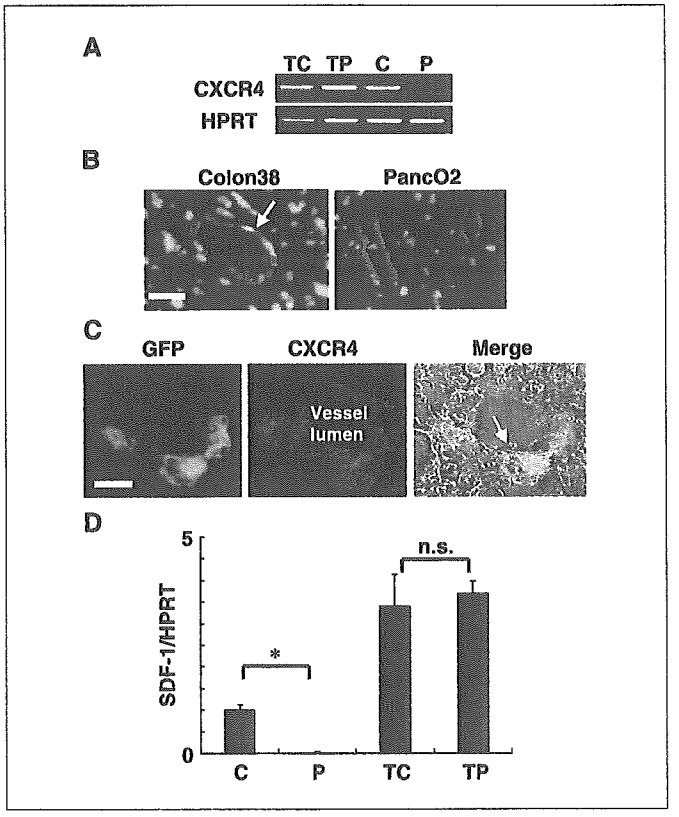

Figure 1. CXCR4-positive cells in s.c. colon and pancreatic tumor tissues. *A*, expression of CXCR4 mRNA was commonly detected by RT-PCR in TICs and in cultured Colon38 cells but not in cultured PancO2 cells. *TC*, TICs from Colon38 tumors; *TP*, TICs from PancO2 tumors; *C*, cultured Colon38 cells; *P*, cultured PancO2 cells. *B*, Colon38 (*left*) and PancO2 (*right*) tumor tissues were stained with anti-CXCR4 (*green*) and anti-CD31 (*red*) antibodies. CXCR4-positive cells were observed around the tumor vessels, and some lined the endothelium (*arrow*). *Bar*, 20 μm. *C*, Colon38 tumor tissues from GFP-BMT mice were stained with anti-CXCR4 antibody. GFP and CXCR4 double-positive cells were found around the tumor vessels (*right, arrow*). *Right*, merged image of differential interference contrast images, GFP (*green*) and CXCR4 (*red*). *Bar*, 20 μm. *D*, total RNA was isolated from s.c. tissues and the two cell lines, and the expression of SDF-1 was analyzed by quantitative RT-PCR.

number per square millimeter using fluorescence microscopy ($n = 3$). GFP and CXCR4 double-positive cells constituted ~3.4% (32.3 ± 2.1 versus 961.3 ± 36.8) or 2.1% (65.7 ± 4.6 versus 3185.7 ± 149.8) of all bone marrow–derived cells in Colon38-derived or PancO2-derived tumors, respectively. For a while, SDF-1 was detected in the extracellular portion of the stromal area, especially around the vessels in both Colon38-derived and PancO2-derived tumors (data not shown). To quantify the expression of SDF-1, we extracted total RNA from s.c. tissues and the two cell lines and did quantitative RT-PCR (Fig. 1*D*). The expression of SDF-1 was induced in both tumor tissues. PancO2 cells did not express SDF-1 *in vitro*; nevertheless, the level of SDF-1 expression in s.c. tumors was not very different from that in Colon38. These findings suggest that SDF-1 is secreted from noncancerous tissues in the tumors or expression could be up-regulated in the tumor tissues. Therefore, the SDF-1/CXCR4 axis seems to contribute to the establishment of tumor tissues via the expression of CXCR4 on infiltrating cells regardless of whether the cancer cells themselves express CXCR4.

CXCR4 neutralization prevents the growth of Colon38 and PancO2 tumors regardless of CXCR4 expression by the cancer cells. We evaluated the therapeutic potential of the neutralization

of CXCR4 for the inhibition of tumor formation using the tumor transplant model. To interfere with SDF-1/CXCR4 signaling, BALB/c nude mice transplanted with Colon38 and PancO2 cells were treated with anti-CXCR4-neutralizing antibody or a control antibody using the dose schedule described in a previous report (32). The growth of Colon38 xenograft tumors was clearly suppressed in the group treated with the neutralizing antibody compared with the control group (n = 5; Fig. 2*A*). Neutralizing antibody against CXCR4 also suppressed the growth of PancO2 tumors (n = 5; Fig. 2*B*). This finding was reproduced in the experiment using C57BL/6 mice. As shown in Fig. 2*C*, neutralizing antibody against CXCR4 also suppressed the growth of Colon38 tumors in C57BL/6 mice (n = 4). As Colon38 cells had been shown to express CXCR4 (Fig. 1*A*), we examined whether the anti-CXCR4-neutralizing antibody could directly inhibit their growth. Colon38 cells were cultured in the presence of 10 μg/mL anti-CXCR4 antibody or control antibody to simulate the concentration in the peripheral blood of treated mice. Under these *in vitro* conditions, anti-CXCR4 antibody treatment had no effect on the growth of Colon38 cells (n = 3; P = 0.93; Fig. 2*D*). To confirm that the effect was independent of the CXCR4 expression by cancer cells themselves, we established Colon38-siCXCR4 cells in which the *CXCR4* gene was stably suppressed. As shown in Fig. 2*E*, the siCXCR4 effectively blocked CXCR4 mRNA expression. Colon38-siCXCR4 cells or Colon38-siRenilla cells were transplanted s.c. into mice and the difference in growth rates was compared. As shown in Fig. 2*G*, growth rates were not significantly different between the two groups (n = 5; P > 0.1). Growth rates were also similar in the *in vitro* culture experiments (Fig. 2*F*).

In addition, we investigated whether the neutralizing antibody has other biological effects *in vitro*, because the SDF-1/CXCR4 axis is significant in breast and colon cancer metastasis. Obvious cytoskeletal changes were not detected by fluorescent phalloidin staining of groups of the two cell lines stained with anti-CXCR4

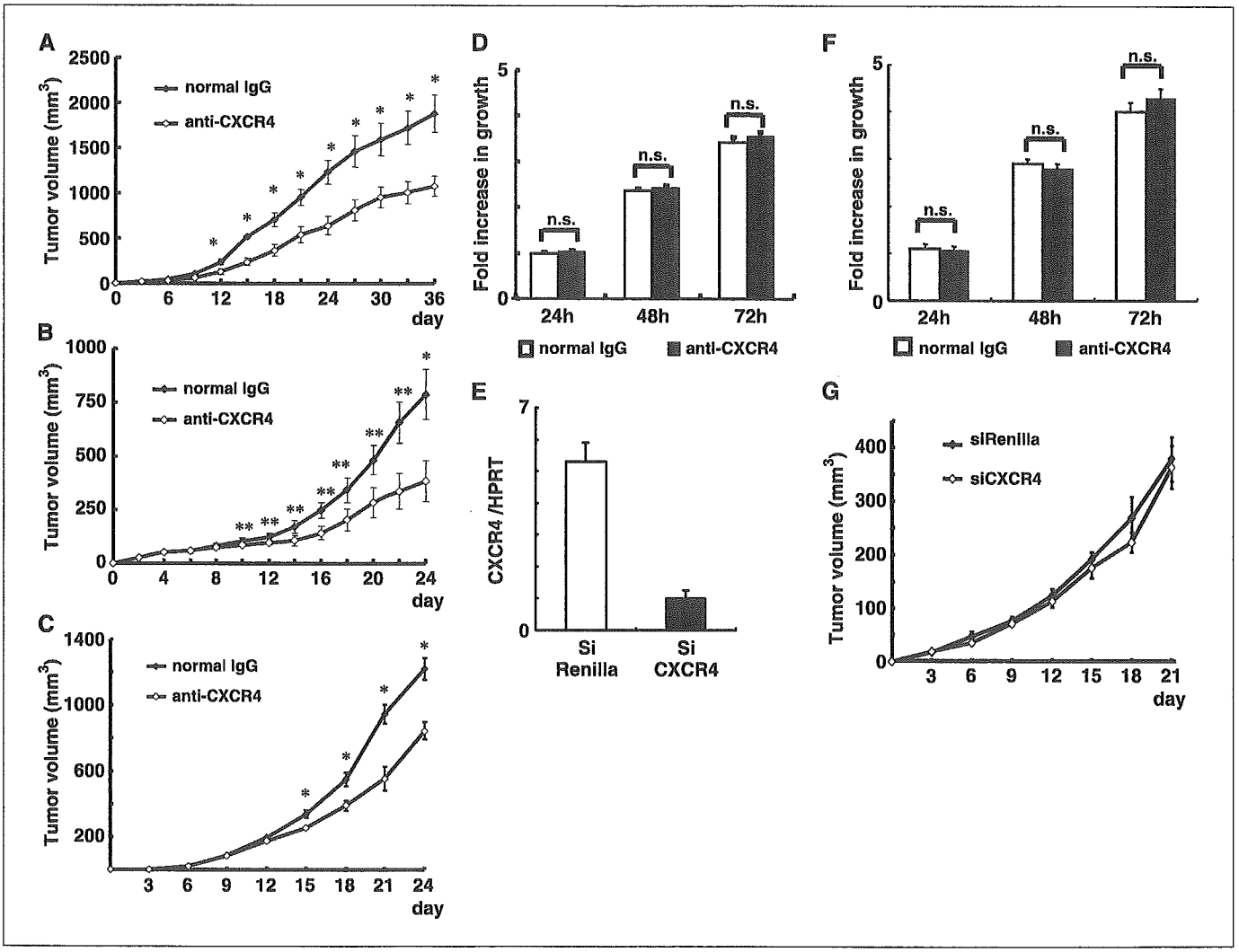

Figure 2. CXCR4 neutralization blocked the growth of s.c. tumors derived from Colon38 and Panco2 cells. BALB/c nude mice were s.c. inoculated with 8 × 10^6 tumor cells. Mice were injected i.p. with anti-CXCR4-neutralizing antibody (10 μg/injection) or with control normal IgG (10 μg/injection) every 24 hours for a total of eight separate injections. Neutralizing antibody against CXCR4 suppressed the growth of tumors derived from Colon38 (*A*) and PancO2 (*B*) cells (n = 5). *Points*, mean; *bars*, SE. *, P < 0.05; **, P < 0.005 (Student's t test). *C*, neutralizing antibody against CXCR4 also suppressed the growth of Colon38 tumors in C57BL/6 mice (n = 4). *D*, anti-CXCR4 antibody treatment had no effect on the growth of cultured Colon38 cells (n = 3; P = 0.93). *n.s.*, not significant. *E*, Colon38 cells were stably transfected with pcPUR+U6-siCXCR4 or pcPUR+U6-siRenilla (control); then, quantitative RT-PCR was done to confirm the CXCR4 mRNA suppression. *F*, growth rates of Colon38-siCXCR4 or Colon38-siRenilla cells were also similar in the *in vitro* culture experiments. *G*, Colon38-siCXCR4 and Colon38-siRenilla cells were transplanted s.c. and the difference in their growth rates was compared (n = 5). *Points*, mean; *bars*, SE.

antibody and control antibody (data not shown). To examine whether the anti-CXCR4-neutralizing antibody treatment affects cell migration, we did a cell migration assay (wound closure assay). No difference in cell migration was observed between the groups for either cell line (data not shown). Between the two groups for both cell lines, there was no statistical difference in the mRNA expression of ICAM ($n = 4$; $P > 0.1$), VCAM ($n = 4$; $P > 0.1$), PDGF ($n = 4$; $P > 0.1$), PlGF ($n = 4$; $P > 0.1$), bFGF ($n = 4$; $P > 0.1$), or MMP-9 ($n = 4$; $P > 0.1$). The VEGF secretion of the Panco2 cells *in vitro* was not statistically different between the two groups ($n = 4$; $P = 0.92$). VEGF production was not detected in the Colon38 cell line. These findings indicate that the suppression of tumor growth was not mediated by the direct inhibition of cancer cell growth.

CXCR4 neutralization decreases the development of tumor endothelium *in vivo*. As CXCR4-positive cells were detected among endothelial cells as well as in the perivascular area (Fig. 1*B*), the effect of CXCR4 neutralization on tumor angiogenesis was estimated by histologic examination of tumors for CD31, an endothelial marker (Fig. 3*A*). The capillary density was calculated as the number of capillaries per square millimeter exhibiting expression of CD31 based on counts in 10 randomly selected fields from each tissue preparation examined by confocal microscopy. Staining with anti-CD31 antibody showed that the density of vessels in the tumors of the mice treated with the neutralizing antibody was significantly lower than that in the tumors of the control group ($n = 3$; $P = 0.00048$; Fig. 3*B*). In addition, the Colon38-siCXCR4 or Colon38-siRenilla cells were transplanted into mice s.c.

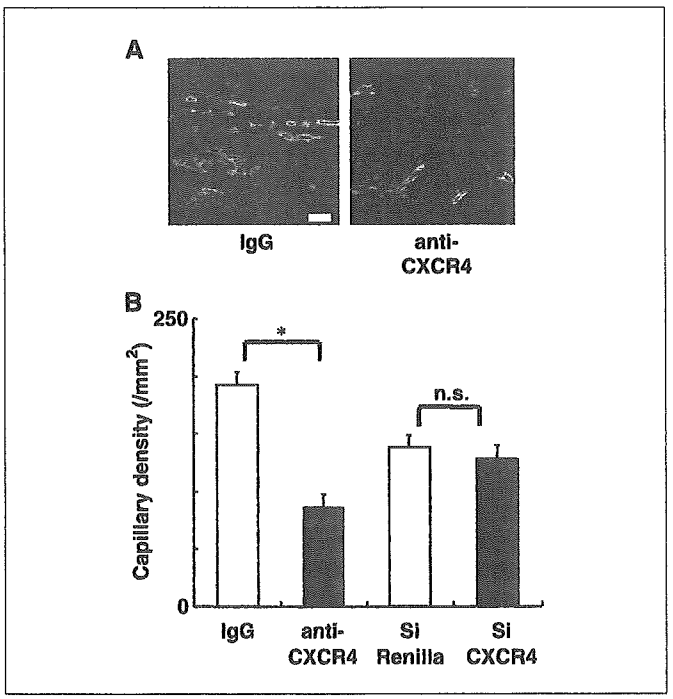

Figure 3. CXCR4 neutralization decreased tumor vessel densities. C57BL/6 mice were injected s.c. with 2×10^6 Colon38 cells. After 1 week, the mice ($n = 3$) were injected i.p. with 10 μg anti-CXCR4-neutralizing antibody or 10 μg normal rabbit IgG (control group). *A*, representative images of CD31 immunostaining after a total of five separate antibody injections. *Bar*, 50 μm. *B*, capillary density was calculated as the number of capillaries per square millimeter based on the counts of 10 randomly selected fields. Treatment with anti-CXCR4 antibody decreased tumor vessel densities (*right*) compared with the control group (*left*). *Columns*, mean ($n = 3$); *bars*, SE. *, $P < 0.05$ (Student's *t* test). The capillary densities in the tumors derived from Colon38-siCXCR4 cells or Colon38-siRenilla cells were not significantly different ($n = 3$; $P = 0.51$).

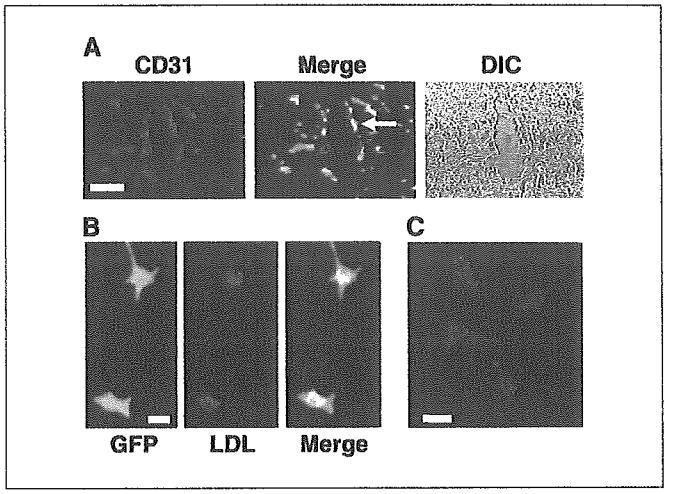

Figure 4. Bone marrow–derived endothelial cells were analyzed *ex vivo* and *in vivo*. *A*, histologic sections of Colon38 tumors from GFP-BMT mice were stained with anti-CD31 antibody (*red*) to detect bone marrow–derived endothelial cells. GFP-positive cells (*green*) rimmed by CD31-positive margins are seen in the tumor endothelium (*arrow*). *Bar*, 20 μm. *B*, PBMCs were analyzed using the late-outgrowth endothelial colony assay. Endothelial cells positive for both DiI-Ac-LDL (*LDL*; *red*) and GFP (*green*) were detected in peripheral blood. *Bar*, 10 μm. *C*, late-outgrowth endothelial cells expressed CXCR4 (*red*). *Bar*, 20 μm.

and the vascularity of the tumors was compared. The capillary densities in the tumors in the two groups were not significantly different ($n = 3$; $P = 0.51$; Fig. 3*B*). Recently, bone marrow–derived endothelial cells were reported to be involved in tumor angiogenesis in tumor implantation models (16–18, 37). To investigate whether bone marrow–derived endothelial cells formed the tumor vessel endothelium in our model, the expression of GFP in the endothelium of the tumor xenografts in GFP-BMT mice was analyzed. GFP and CD31 double-positive cells were observed lining the vessels only in rare instances, suggesting that the population of bone marrow–derived tumor endothelial cells was very limited in our model (Fig. 4*A*). The presence of endothelial progenitor cells in the peripheral blood of tumor-bearing mice was investigated using the late-outgrowth assay. PBMCs were cultured to permit the growth of endothelial colonies, which were then identified by the metabolic uptake of DiI-Ac-LDL after 2 weeks of culture. The expression of GFP was detected in most of the DiI-Ac-LDL-positive colonies (Fig. 4*B*), but these cells did not form large colonies under our experimental conditions. Importantly, late-outgrowth cells identified *in vitro* expressed the chemokine receptor CXCR4 (Fig. 4*C*).

***In vivo* neutralization of CXCR4 decreases the intratumor blood flow.** As the blockade of CXCR4 induced a decrease in the development of intratumor endothelial cells, we monitored dynamic changes in the blood perfusion of the tumors using a LDPI system (35, 36). LDPI can provide noninvasive analysis of local perfusion in superficial tissues. The technique is based on the principle that the wavelength of laser light changes (Doppler shift) when it is reflected from a moving object (RBC in this case), whereas the wavelength of light reflected from a stationary object remains unchanged. The Doppler-shifted light is converted into an arbitrary perfusion signal, which is approximately proportional to the mean blood cell velocity multiplied by the concentration of moving blood cells (Fig. 5*A*). The blood flow in the tumors treated with neutralizing antibody was decreased to ~65% of that in the control tumors for both s.c. Colon38 and PancO2 tumors ($n = 7$; $P < 0.01$ and

$P < 0.001$, respectively; Fig. 5*B*). Taken together with the observations presented in Fig. 2, these findings indicate that neutralization of CXCR4 suppresses tumor growth by an antiangiogenic mechanism and not by direct inhibition of cell growth. In addition, the Colon38-siCXCR4 or Colon38-siRenilla cells were transplanted into mice s.c. The Doppler flow rates in the tumors were similar ($n = 5$; $P = 0.57$; Fig. 5*B*). These results indicate that the decrease in tumor vascularity with anti-CXCR4 neutralizing antibodies is not caused by a direct effect against cancer cells.

CXCR4 neutralization did not change vascular endothelial growth factor expression in the tumor tissues or induce critical anemia. Cells of inflammatory cell lineages that infiltrate into tumors have been reported to secrete VEGF, a pivotal angiogenic factor (38, 39). By immunohistochemistry, some of the infiltrated cells were Mac3 positive, which indicated that monocytes/macrophages had been recruited into the tumor tissues from the bone marrow (Fig. 6*A*). In a short time, few anti–smooth muscle actin–positive cells were detected in our analysis (data not shown), which might be consistent with reports that tumor microvessels often lack a lining of smooth muscle cells unlike normal vessels. To determine whether the TICs secrete VEGF in our xenograft tumor model, we counterstained the GFP-positive cells of Colon38 tumor with anti-VEGF antibody. As shown in Fig. 6*B*, VEGF was expressed in the GFP-positive, bone marrow–derived infiltrating cells in our xenograft tumors (Fig. 6*B*). To clarify the effect of blocking CXCR4 on VEGF expression, the VEGF concentrations in the tumors were determined using ELISA and compared between the groups treated with CXCR4-neutralizing antibody and control antibodies. As shown in Fig. 6*C*, the VEGF concentration was not significantly affected by CXCR4 neutralization. These findings suggest that the suppression of angiogenesis by the neutralization of CXCR4 is not attributable to a change in the VEGF concentration and that VEGF secretion does not always depend on CXCR4-positive TICs. Indeed, the blockade of CXCR4 did not cause a major change in the number of perivascular bone marrow–derived GFP-positive cells in the tumor tissues (Fig. 6*D*). Inflammatory cells that infiltrate tumors have been reported to express various angiogenic factors. It has been suggested that the cells producing vascular mitogens can be mobilized by other mechanisms independent of SDF-1/CXCR4 signaling. Furthermore, because the SDF-1/CXCR4 axis is indispensable for hematopoietic stem cell homing (8), the inhibition of this interaction might impair bone marrow hematopoiesis. To exclude the possibility that the decrease in tumor perfusion measured in mice treated with CXCR4-neutralizing antibody was caused by anemia, which can result in the underestimation of intratumor blood flow by the LDPI system, the peripheral blood cell counts were determined for each

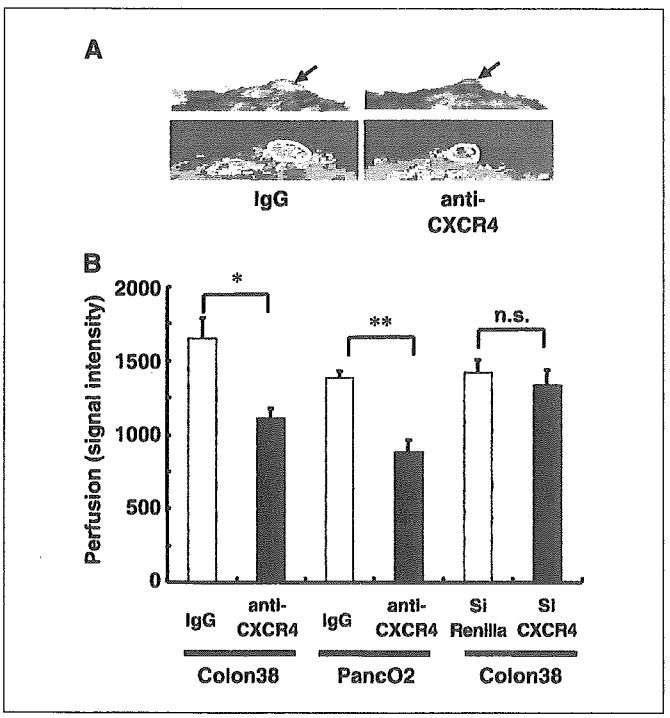

Figure 5. CXCR4 neutralization decreased the intratumor blood flow *in vivo*. *A*, representative images of blood flow in tumor tissues from the LDPI system. *Arrow*, s.c. tumor (*top*). The average flow in closed areas was measured as the intratumor blood flow (*bottom*). *B*, blood flow in s.c. Colon38 and PancO2 tumors treated with CXCR4-neutralizing antibody was decreased in comparison with the control tumors ($n = 7$). *, $P < 0.01$; **, $P < 0.001$. The blood flow in s.c. Colon38-siCXCR4-derived or Colon38-siRenilla-derived tumors was also estimated ($n = 5$; $P > 0.5$).

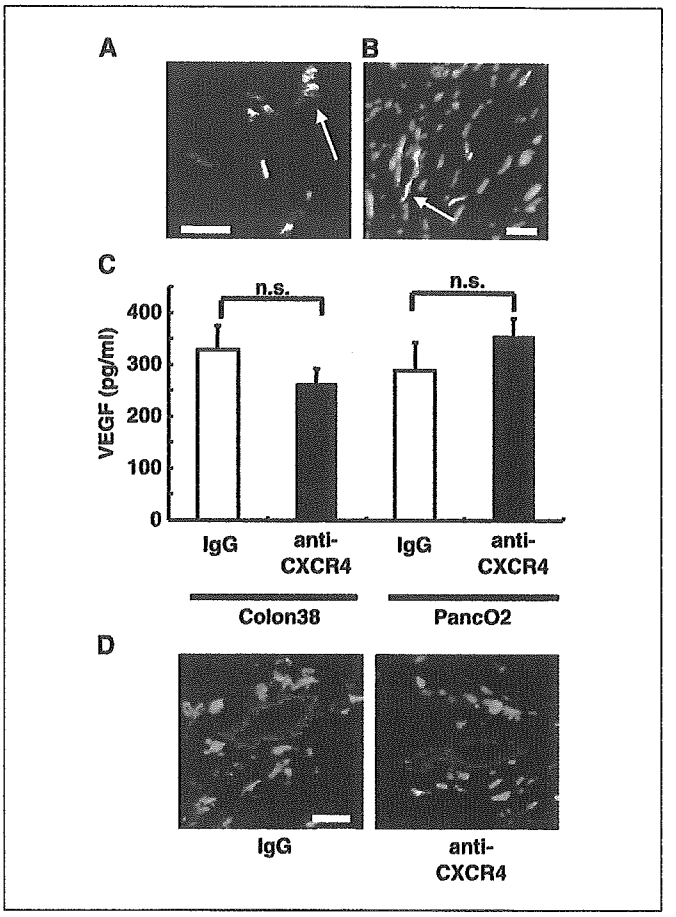

Figure 6. Neutralization of CXCR4 did not change the VEGF concentration in the Colon38 and PancO2 tumors. *A*, Colon38 tumor tissue of GFP-BMT mice was immunostained with anti-Mac3 antibody. Some of the GFP-positive infiltrating cells were Mac3 positive (*arrow*). *Bar*, 10 μm. *B*, Colon38 tumor of GFP-BMT mice was counterstained with anti-VEGF antibody. VEGF expression (*red*) was seen in the GFP-positive, bone marrow–derived infiltrating cells in our xenograft tumors (*arrow*), *Bar*, 10 μm. *C*, concentration of VEGF was determined by ELISA assay in the tumors on day 14 following five antibody injections and was compared between the groups treated with anti-CXCR4-neutralizing antibody and with control antibodies ($n = 7$). *D*, no major change in the number of perivascular bone marrow–derived GFP-positive cells in the tumor tissues treated with CXCR4 blockade compared with control tumors. *Red*, CD31-positive endothelial cells. *Bar*, 20 μm.

group (Table 1). The peripheral blood cell counts were not significantly different between the groups, which indicated that CXCR4 antibody did not induce a critical suppression of the bone marrow under our experimental conditions.

Discussion

In this study, we showed that the SDF-1/CXCR4 axis, which is indispensable for hematopoiesis and angiogenesis in the embryo (20, 40), plays a pivotal role in tumor progression through promoting tumor neovascularization. Our findings might provide new insight on the significance of the SDF-1/CXCR4 axis in local tumor progression. The reported ability of CXCR4 neutralization to block the growth of metastatic lesions might be mediated in part by this inhibition of angiogenesis. Although this antigrowth effect is independent of CXCR4 expression by cancer cells, based on the results of small interfering RNA experiments, this does not contradict the recent reports that *in vivo* breast cancer growth was dependent on CXCR4 (41). The significance of the SDF-1/CXCR4 axis for cancer cell growth *in vivo* could differ by cancer cell type. For example, the CXCR4 expression of gastrointestinal tumors might be less than that of breast cancer. In addition, another mitogenic signaling pathway could compensate for the growth disadvantage by inhibiting the SDF-1/CXCR4 axis in gastrointestinal tumors. Indeed, oncogenic mutations of the *K-Ras* or *B-Raf* genes that strongly induce hyperproliferative capacity are often reported in gastrointestinal tumors. Importantly, the anticancer potential of the CXCR4-blocking strategy may be effective for a broad spectrum of cancers.

During tumor progression, infiltrating cells produce several potent angiogenic growth factors, cytokines, and proteases (38, 39). The recruitment and infiltration of circulating cells are mediated by members of the chemokine family of chemoattractive cytokines. In our murine tumor models, the neutralization of CXCR4 did not change the concentration of VEGF in the tumors, suggesting that other chemokine systems function in the recruitment of VEGF-secreting cells. Although the capillary density was lower in anti-CXCR4-treated tumors in spite of unchanged VEGF concentrations, our data do not exclude the significance of VEGF in tumor angiogenesis. Our results indicate that the SDF-1/CXCR4 axis does not always regulate tumor angiogenesis in a VEGF-dependent manner; for example, the SDF-1/CXCR4 axis might contribute to functional vascular establishment by the regulation of endothelial tube formation (1).

Recently, circulating endothelial progenitor cells mobilized from bone marrow have been detected in the peripheral blood of several species and shown to be involved in neoangiogenesis in tumors as well as in the formation of new vessels after trauma, burn injury, and myocardial infarction (16–18). We have already documented the roles of bone marrow–derived vascular progenitor cells in vascular remodeling using the original reconstituted bone marrow mouse model (27, 30). In the present study using Colon38 and Panco2 cells, bone marrow–derived endothelial cells were infrequently detected in the capillaries of the tumors. However, our findings do not exclude the possibility that SDF-1/CXCR4 axis neutralization inhibits bone marrow–dependent tumor vasculogenesis, as is the case for embryonic vasculogenesis (42), because peripheral blood–derived late-outgrowth colonies expressed CXCR4 (Fig. 4*C*; ref. 43). The proportion of bone marrow–derived endothelial cells incorporated during neovascularization might differ among tumor types (44, 45) or might be influenced by the local expression profiles of various cytokines or growth factors (46). A recent study reported that *in vivo* expression of SDF-1 in ischemic tissues and CXCR4-positive progenitor recruitment were enhanced by the transcription factor hypoxia-inducible factor-1 (HIF-1; ref. 47). In another report, the metastatic ability of cancer cells was regulated by HIF-1-dependent CXCR4 expression (48). These findings suggest that HIF-1 expression in tumors might affect the recruitment of CXCR4-positive endothelial progenitors. Therefore, the degree of angiogenic inhibition by CXCR4 neutralization might increase in proportion to the contribution made by the recruitment of bone marrow–derived CXCR4-positive progenitors. Further experiments should be conducted in tumors of different origins to analyze the variation in the contribution of bone marrow–dependent vasculogenesis to tumor angiogenesis and the antitumor effects of the blockade of CXCR4.

Inhibitors of angiogenesis, such as anti-VEGF antibody, are expected to be able to suppress the advancement of tumor growth (49, 50). Treatment with bevacizumab, a monoclonal antibody against VEGF, in combination with fluorouracil/leucovorin treatment resulted in higher response rates and longer median survival times than treatment with fluorouracil/leucovorin alone (51). Moreover, because neovascularization processes are not continuously active in adult tissues, the targeting of vasculogenic reactions would be a relatively tumor-specific therapy (52). In contrast to the strategies employed by many anticancer drugs, strategies that target specific molecules might induce selective effects against cancer tissues. For example, the actions and interactions of endothelial cells and pericytes in tumors are qualitatively different from those in normal tissues (53), which might permit the specific targeting of the tumor vasculature. Indeed, SU6668, an inhibitor of VEGF and PDGF receptors, disrupted the association of pericytes with endothelium and reduced the vascularity in tumor tissues only (54).

Our experiments showed that injection of anti-CXCR4 antibody caused no critical bone marrow suppression or ischemic event.

Table 1. Peripheral blood cell counts in mice treated with normal IgG or anti-CXCR4 antibody

Treatment	Cancer cell type	RBC ($\times$10,000/mm^3)	Hemoglobin (g/dL)	WBC (/μL)
Normal IgG	Colon38	878 $\pm$ 33	14.3 $\pm$ 0.52	3367 $\pm$ 376
Anti-CXCR4	Colon38	901 $\pm$ 28^{NS}	14.5 $\pm$ 0.35^{NS}	3200 $\pm$ 173^{NS}
Normal IgG	PancO2	802 $\pm$ 46	14.2 $\pm$ 0.18	2233 $\pm$ 376
Anti-CXCR4	PancO2	853 $\pm$ 38^{NS}	13.8 $\pm$ 0.45^{NS}	3133 $\pm$ 286^{NS}

NOTE: Peripheral blood cells were counted on day 14 after tumor inoculation (n = 3 for each group). NS, not significantly different versus normal IgG-treated mice.

Based on our data, the inhibition of vasculogenesis by CXCR4 neutralization might be cooperatively effective against tumors in combination with other angiogenic inhibitors, such as anti-VEGF antibody or chemotherapeutic drugs. In the future, combined strategies that include targeting SDF-1/CXCR4 might be promising anticancer therapies against a broad spectrum of cancers.

Acknowledgments

Received 10/25/2004; revised 3/16/2005; accepted 4/22/2005.

The costs of publication of this article were defrayed in part by the payment of page charges. This article must therefore be hereby marked *advertisement* in accordance with 18 U.S.C. Section 1734 solely to indicate this fact.

We thank Mitsuko Tsubouchi and members of the Sata Laboratory for their technical assistance.

References

1. Salvucci O, Yao L, Villalba S, Sajewicz A, Pittaluga S, Tosato G. Regulation of endothelial cell branching morphogenesis by endogenous chemokine stromal-derived factor-1. Blood 2002;99:2703–11.
2. Muller A, Homey B, Soto H, et al. Involvement of chemokine receptors in breast cancer metastasis. Nature 2001;410:50–6.
3. Federsppiel B, Melhado IG, Duncan AM, et al. Molecular cloning of the cDNA and chromosomal localization of the gene for a putative seven-transmembrane segment (7-TMS) receptor isolated from human spleen. Genomics 1993;16:707–12.
4. Baggiolini M. Chemokines and leukocyte traffic. Nature 1998;392:565–8.
5. Volin MV, Joseph L, Shockley MS, Davies PF. Chemokine receptor CXCR4 expression in endothelium. Biochem Biophys Res Commun 1998;242:46–53.
6. Feil C, Augustin HG. Endothelial cells differentially express functional CXC-chemokine receptor-4 (CXCR-4/fusin) under the control of autocrine activity and exogenous cytokines. Biochem Biophys Res Commun 1998;247:38–45.
7. Ganju RK, Brubaker SA, Meyer J, et al. The α-chemokine, stromal cell-derived factor-1α, binds to the transmembrane G-protein-coupled CXCR-4 receptor and activates multiple signal transduction pathways. J Biol Chem 1998;273:23169–75.
8. Ara T, Tokoyoda K, Sugiyama T, Egawa T, Kawabata K, Nagasawa T. Long-term hematopoietic stem cells require stromal cell-derived factor-1 for colonizing bone marrow during ontogeny. Immunity 2003;19:257–67.
9. Bachelder RE, Wendt MA, Mercurio AM. Vascular endothelial growth factor promotes breast carcinoma invasion in an autocrine manner by regulating the chemokine receptor CXCR4. Cancer Res 2002;62:7203–6.
10. Zeelenberg IS, Ruuls-Van Stalle L, Roos E. The chemokine receptor CXCR4 is required for outgrowth of colon carcinoma micrometastases. Cancer Res 2003;63:3833–9.
11. Kang Y, Siegel PM, Shu W, et al. A multigenic program mediating breast cancer metastasis to bone. Cancer Cell 2003;3:537–49.
12. Lee BC, Lee TH, Avraham S, Avraham HK. Involvement of the chemokine receptor CXCR4 and its ligand stromal cell-derived factor 1α in breast cancer cell migration through human brain microvascular endothelial cells. Mol Cancer Res 2004;2:327–38.
13. Libura J, Drukala J, Majka M, et al. CXCR4-SDF-1 signaling is active in rhabdomyosarcoma cells and regulates locomotion, chemotaxis, and adhesion. Blood 2002;100:2597–606.
14. Robledo MM, Bartolome RA, Longo N, et al. Expression of functional chemokine receptors CXCR3 and CXCR4 on human melanoma cells. J Biol Chem 2001;276:45098–105.
15. Murakami T, Maki W, Cardones AR, et al. Expression of CXC chemokine receptor-4 enhances the pulmonary metastatic potential of murine B16 melanoma cells. Cancer Res 2002;62:7328–34.
16. Asahara T, Masuda H, Takahashi T, et al. Bone marrow origin of endothelial progenitor cells responsible for postnatal vasculogenesis in physiological and pathological neovascularization. Circ Res 1999;85:221–8.
17. Lyden D, Hattori K, Dias S, et al. Impaired recruitment of bone-marrow-derived endothelial and hematopoietic precursor cells blocks tumor angiogenesis and growth. Nat Med 2001;7:1194–201.
18. Gill M, Dias S, Hattori K, et al. Vascular trauma induces rapid but transient mobilization of VEGFR2(+)AC133(+) endothelial precursor cells. Circ Res 2001;88:167–74.
19. McGrath KE, Koniski AD, Maltby KM, McGann JK, Palis J. Embryonic expression and function of the chemokine SDF-1 and its receptor, CXCR4. Dev Biol 1999;213:442–56.
20. Tachibana K, Hirota S, Iizasa H, et al. The chemokine receptor CXCR4 is essential for vascularization of the gastrointestinal tract. Nature 1998;393:591–4.
21. Takakura N, Watanabe T, Suenobu S, et al. A role for hematopoietic stem cells in promoting angiogenesis. Cell 2000;102:199–209.
22. Okabe M, Ikawa M, Kominami K, Nakanishi T, Nishimune Y. "Green mice" as a source of ubiquitous green cells. FEBS Lett 1997;407:313–9.
23. Tsuruo T, Yamori T, Tsukagoshi S, Sakurai Y. Enhanced cytocidal action of methotrexate by conjugation to concanavalin A. Int J Cancer 1980;26:655–9.
24. Morikane K, Tempero RM, Sivinski CL, et al. Organ-specific pancreatic tumor growth properties and tumor immunity. Cancer Immunol Immunother 1999;47:287–96.
25. Miyagishi M, Taira K. U6 promoter-driven siRNAs with four uridine 3′ overhangs efficiently suppress targeted gene expression in mammalian cells. Nat Biotechnol 2002;20:497–500.
26. Jazag A, Ijichi H, Kanai F, et al. Smad4 silencing in pancreatic cancer cell lines using stable RNA interference and gene expression profiles induced by transforming growth factor-β. Oncogene 2005;24:662–71.
27. Sata M, Saiura A, Kunisato A, et al. Hematopoietic stem cells differentiate into vascular cells that participate in the pathogenesis of atherosclerosis. Nat Med 2002;8:403–9.
28. Radoja S, Saio M, Schaer D, Koneru M, Vukmanovic S, Frey AB. CD8(+) tumor-infiltrating T cells are deficient in perforin-mediated cytolytic activity due to defective microtubule-organizing center mobilization and lytic granule exocytosis. J Immunol 2001;167:5042–51.
29. Wright DE, Bowman EP, Wagers AJ, Butcher EC, Weissman IL. Hematopoietic stem cells are uniquely selective in their migratory response to chemokines. J Exp Med 2002;195:1145–54.
30. Tanaka K, Sata M, Hirata Y, Nagai R. Diverse contribution of bone marrow cells to neointimal hyperplasia after mechanical vascular injuries. Circ Res 2003;93:783–90.
31. Tateishi K, Omata M, Tanaka K, Chiba T. The NEDD8 system is essential for cell cycle progression and morphogenetic pathway in mice. J Cell Biol 2001;155:571–9.
32. Petit I, Szyper-Kravitz M, Nagler A, et al. G-CSF induces stem cell mobilization by decreasing bone marrow SDF-1 and up-regulating CXCR4. Nat Immunol 2002;3:687–94.
33. Kanai F, Kawakami T, Hamada H, et al. Adenovirus-mediated transduction of *Escherichia coli* uracil phosphoribosyltransferase gene sensitizes cancer cells to low concentrations of 5-fluorouracil. Cancer Res 1998;58:1946–51.
34. Abbott JD, Huang Y, Liu D, Hickey R, Krause DS, Giordano FJ. Stromal cell-derived factor-1α plays a critical role in stem cell recruitment to the heart after myocardial infarction but is not sufficient to induce homing in the absence of injury. Circulation 2004;110:3300–5.
35. Crosby JR, Kaminski WE, Schatteman G, et al. Endothelial cells of hematopoietic origin make a significant contribution to adult blood vessel formation. Circ Res 2000;87:728–30.
36. Schlingemann RO, Rietveld FJ, de Waal RM, Ferrone S, Ruiter DJ. Expression of the high molecular weight melanoma-associated antigen by pericytes during angiogenesis in tumors and in healing wounds. Am J Pathol 1990;136:1393–405.
37. Asahara T, Murohara T, Sullivan A, et al. Isolation of putative progenitor endothelial cells for angiogenesis. Science 1997;275:964–7.
38. Coussens LM, Werb Z. Inflammation and cancer. Nature 2002;420:860–7.
39. Carmeliet P. Mechanisms of angiogenesis and arteriogenesis. Nat Med 2000;6:389–95.
40. Zou YR, Kottmann AH, Kuroda M, Taniuchi I, Littman DR. Function of the chemokine receptor CXCR4 in haematopoiesis and in cerebellar development. Nature 1998;393:595–9.
41. Smith MC, Luker KE, Garbow JR, et al. CXCR4 regulates growth of both primary and metastatic breast cancer. Cancer Res 2004;64:8604–12.
42. Carmeliet P. Angiogenesis in health and disease. Nat Med 2003;9:653–60.
43. Yamaguchi J, Kusano KF, Masuo O, et al. Stromal cell-derived factor-1 effects on *ex vivo* expanded endothelial progenitor cell recruitment for ischemic neovascularization. Circulation 2003;107:1322–8.
44. Ruzinova MB, Schoer RA, Gerald W, et al. Effect of angiogenesis inhibition by Id loss and the contribution of bone-marrow-derived endothelial cells in spontaneous murine tumors. Cancer Cell 2003;4:277–89.
45. Sikder H, Huso DL, Zhang H, et al. Disruption of Id1 reveals major differences in angiogenesis between transplanted and autochthonous tumors. Cancer Cell 2003;4:291–9.
46. Takahashi T, Kalka C, Masuda H, et al. Ischemia- and cytokine-induced mobilization of bone marrow-derived endothelial progenitor cells for neovascularization. Nat Med 1999;5:434–8.
47. Ceradini DJ, Kulkarni AR, Callaghan MJ, et al. Progenitor cell trafficking is regulated by hypoxic gradients through HIF-1 induction of SDF-1. Nat Med 2004;10:858–64.
48. Staller P, Sulitkova J, Lisztwan J, Moch H, Oakeley EJ, Krek W. Chemokine receptor CXCR4 downregulated by von Hippel-Lindau tumour suppressor pVHL. Nature 2003;425:307–11.
49. Kerbel R, Folkman J. Clinical translation of angiogenesis inhibitors. Nat Rev Cancer 2002;2:727–39.
50. Willett CG, Boucher Y, di Tomaso E, et al. Direct evidence that the VEGF-specific antibody bevacizumab has antivascular effects in human rectal cancer. Nat Med 2004;10:145–7.
51. Kabbinavar F, Hurwitz HI, Fehrenbacher L, et al. Phase II, randomized trial comparing bevacizumab plus fluorouracil (FU)/leucovorin (LV) with FU/LV alone in patients with metastatic colorectal cancer. J Clin Oncol 2003;21:60–5.
52. Carmeliet P, Moons L, Luttun A, et al. Synergism between vascular endothelial growth factor and placental growth factor contributes to angiogenesis and plasma extravasation in pathological conditions. Nat Med 2001;7:575–83.
53. Jain RK. Determinants of tumor blood flow: a review. Cancer Res 1988;48:2641–58.
54. Bergers G, Song S, Meyer-Morse N, Bergsland E, Hanahan D. Benefits of targeting both pericytes and endothelial cells in the tumor vasculature with kinase inhibitors. J Clin Invest 2003;111:1287–95.

p53-Independent Negative Regulation of p21/Cyclin-Dependent Kinase–Interacting Protein 1 by the Sonic Hedgehog-Glioma-Associated Oncogene 1 Pathway in Gastric Carcinoma Cells

Miki Ohta,[1,4] Keisuke Tateishi,[1] Fumihiko Kanai,[1,5] Hirotsugu Watabe,[1] Shintaro Kondo,[1] Bayasi Guleng,[1] Yasuo Tanaka,[1] Yoshinari Asaoka,[1] Amarsanaa Jazag,[1] Jun Imamura,[1] Hideaki Ijichi,[1] Tsuneo Ikenoue,[1] Masataka Sata,[2] Makoto Miyagishi,[3,6] Kazunari Taira,[3,6] Minoru Tada,[1] Takao Kawabe,[1,4] and Masao Omata[1,4,5]

Departments of [1]Gastroenterology and [2]Cardiovascular Medicine, Graduate School of Medicine and [3]Department of Chemistry and Biotechnology, Graduate School of Engineering, University of Tokyo; [4]Department of Endoscopy and Endoscopic Surgery and [5]Clinical Research Center, University of Tokyo Hospital, Tokyo, Japan; and [6]Gene Discovery Research Center, National Institute of Advanced Industrial Science and Technology, Tsukuba, Japan

Abstract

The activation of Hedgehog (Hh) signaling has been implicated in the growth of various tumor types, including gastric carcinoma. However, the precise mechanisms of Hh activation and suppression of tumor growth by the blockade of Hh signaling in gastric carcinoma cells remain unknown. The aim of this study was to elucidate the mechanism of abnormal Hh signaling and the key molecules contributing to dysregulated growth of gastric carcinoma. The Sonic hedgehog (Shh) ligand and its receptor Patched were expressed in all five gastric carcinoma cell lines examined (MKN1, MKN7, MKN45, MKN74, and AGS cells). The blockade of Hh signaling with anti-Shh antibody inhibited the growth of all five gastric carcinoma cell lines. Shh was overexpressed (mean, 12.8-fold) in 8 of 14 (57.0%) cancerous tissue samples from patients with gastric carcinoma as compared with expression in the surrounding noncancerous tissues. The disruption of glioma-associated oncogene 1 (Gli1) by small interfering RNA induced an increase in p21/cyclin-dependent kinase–interacting protein 1 (CIP1), interfered with the G_1-S transition, and suppressed cell proliferation. The stimulation or inhibition of Hh signaling did not affect p53 activity and the induction of p21/CIP1 expression and the G_1 arrest by inhibition of Hh signaling were not affected by the p53 status. These findings suggest that the overexpression of Shh contributes to constitutive Hh activation and that this signaling pathway negatively regulates p21/CIP1 through a Gli1-dependent and p53-independent mechanism in gastric carcinoma cells. (Cancer Res 2005; 65(23): 10822-9)

Introduction

The Hedgehog (Hh) signaling pathway has indispensable roles in organized cell growth and differentiation in a variety of embryonic tissues, including limbs, the nervous system, and the digestive tract (1–5). Hh signaling is also involved in the maintenance of homeostasis in postembryonic tissues by regulating the fates of stem cells (6, 7). Recent findings have implicated Hh signaling in the growth of various tumors (8, 9), such as basal cell carcinoma (10–12), medulloblastoma (13, 14), small-cell lung cancer (15), digestive tract tumors (16, 17), prostate carcinoma (18, 19), and breast cancer (20).

Hh signaling is transduced by a seven-transmembrane-spanning protein, Smoothened (Smo), the activity of which is suppressed by the receptor Patched (Ptch). Constitutive-activation mutations in the *smo* gene (21) and loss-of-function mutations in the *ptch* gene (10, 22) cause abnormal activation of Hh signaling in a ligand-independent manner in basal cell carcinoma and brain tumors. By contrast, Hh ligand–dependent abnormal activation has also been reported in some digestive tumors and prostate carcinoma (17, 18). Hh signaling is also activated in gastric carcinoma cells (17, 23); however, the molecular mechanisms underlying this abnormal activation remain unclear. Cyclopamine, a steroidal alkaloid that interacts directly with Smo to inhibit Hh signaling, effectively retards the growth of various tumors, including gastric carcinoma, indicating that Hh signaling is involved in tumor growth (15–17, 20). Nevertheless, it remains unclear how the blockade of Hh signaling leads to tumor growth suppression in gastric cancer.

This study examined the mechanism of abnormal Hh signaling in gastric carcinoma cells and sought to identify the key molecules that contribute to tumor cell growth regulated by Hh signaling. We showed that the abnormal Hh signaling in gastric carcinoma cells is caused mainly by the constitutive overexpression of the Sonic hedgehog (Shh) ligand in the cancer cells themselves. Furthermore, our data indicate that the Hh signaling pathway negatively regulates the expression of the cyclin-dependent kinase (CDK) inhibitor p21/CDK-interacting protein 1 (CIP1) in a glioma-associated oncogene 1 (Gli1)–dependent and p53-independent manner. Our findings suggest that Shh-Gli1 signaling contributes to the acceleration of tumor growth through the negative regulation of p21/CIP1 expression in gastric carcinoma cells.

Materials and Methods

Cell lines and human gastric tissue samples. Five human gastric carcinoma cell lines (AGS, MKN1, MKN7, MKN45, and MKN74) and an embryonic kidney cell line (HEK 293T) were purchased from American Type Culture Collection (Manassas, VA) or Japanese Riken Cell Bank (Tsukuba, Japan). Tissue specimens from 14 patients with gastric carcinoma who

Requests for reprints: Keisuke Tateishi, Department of Gastroenterology, University of Tokyo, Hongo 7-3-1, Bunkyo-ku, Tokyo 113-8655, Japan. Phone: 81-3-3815-5411, ext. 33070; Fax: 81-3-3814-0021; E-mail: ktate-tky@umin.ac.jp.

doi:10.1158/0008-5472.CAN-05-0777

underwent gastrectomies were obtained from the archives of Motojima General Hospital, Gumma, Japan, after approval from the medical ethics committee and acquisition of informed consent. The samples of cancerous and noncancerous gastric tissues (the normal tissue surrounding the tumors) had been collected immediately after gastrectomy, frozen in liquid nitrogen, and stored at −80°C. Formalin-fixed, paraffin-embedded sections were examined using H&E staining and immunohistochemistry.

Reagents and blocking antibody. The Smo-specific inhibitor cyclopamine (Toronto Research Chemicals, North York, Ontario, Canada; refs. 16, 24) was dissolved in DMSO. Mouse anti-Shh blocking antibody (5E1; Developmental Studies Hybridoma Bank, University of Iowa, Iowa City, IA) and control mouse immunoglobulin G (IgG; Sigma-Aldrich, St. Louis, MO) were used at the concentrations indicated in the text.

Transfection constructs. The Gli1 expression plasmid pcDNA3/Gli1 (25, 26) and the p53 expression plasmid pCXN2/p53 (27) and the respective empty control plasmids were used. The wild-type Smo expression plasmid was also obtained and the mutated Smo (pGEN/Smo-W539L), which activates the Hh signal pathway without stimulation by Hh ligand, was generated (21, 28). The p53 reporter plasmid containing the *Photinus pyralis* (firefly) luciferase gene was purchased from Stratagene (La Jolla, CA). The pRL-TK control plasmid that expresses the *Renilla reniformis* (sea pansy) luciferase gene driven by the Herpes simplex virus thymidine kinase promoter was also used (Toyo Ink, Tokyo, Japan). The transfection assay was done using FuGene transfection reagent (Roche, Penzberg, Germany) as previously described (19).

Construction and transfection of the vector for Gli1 RNA interference. A plasmid expressing a double-stranded small interfering RNA against the *Gli1* gene was generated from the pcPUR+U6i cassette vector (pcPUR) as previously described (29, 30). Briefly, a sequence targeting the *Gli1* gene was selected and sense and antisense oligonucleotides (5′-CACCGATAGAGCTTTGATCTTTAACGTGTGCTGTCCGTTAAGGATCAAAGTTCTGTCTTTTT-3′ and 5′-GCATAAAAAGACAGAACTTTGATCCTTAACGGACAGCACACGTTAAAGATCAAAGCTCTATC-3′, respectively) were designed to generate a short hairpin RNA. The two oligonucleotides were annealed to each other and inserted into the pcPUR+U6i cassette vector to generate the Gli1 knockdown vector (pc-PUR/siGli1; siGli1). A control pcPUR vector that produces RNA interference against the green fluorescent protein (GFP) gene (pc-PUR/siGFP; siGFP) was also used (29). For transfection, the cells were seeded onto 10-cm dishes and siGli1 or the control vector was added to each dish 24 hours later. The transfected cells were cultured for 24 hours in the appropriate medium containing 2 μg/mL puromycin (Wako, Osaka, Japan) followed by an additional 24 hours in medium without puromycin. Transfected cells were used for proliferation assays, cell cycle analysis, extraction of total cell lysates for immunoblot analysis, and preparation of total RNA for reverse transcription-PCR (RT-PCR) and cDNA arrays.

Immunoblotting and immunohistochemistry. Immunoblotting was done as previously described (31). Mouse anti-Shh (1:1,000), rabbit anti-Gli1 (1:250; Chemicon, Temecula, CA), mouse anti-p21/CIP1 (1:1,000; Transduction Laboratories, Lexington, KY), mouse anti-p27/KIP1 (1:1,000; Transduction Laboratories), rabbit anti-p53 (1:1,000, Santa Cruz Biotechnology, Santa Cruz, CA), and mouse anti-β-actin (1:5,000, Sigma-Aldrich) antibodies were used as the primary labeling antibodies and the appropriate horseradish peroxidase–conjugated antibodies (1:2,000; Amersham, Uppsala, Sweden) were used as secondary antibodies. An enhanced chemiluminescence detection system (ECL-Plus, Amersham) was used for detection.

Immunohistochemistry was done as previously described (16) using anti-Shh (1:100) and anti-Gli1 (1:200) antibodies. For the second antibody, Histofine Simple Stain MAX-PO (Nichirei, Tokyo, Japan), which is an amino acid polymer coated with goat immunoglobulin (Fab′) and peroxidase, was used. Endogenous peroxidase activity was blocked using 3% H_2O_2 for 10 minutes at room temperature. Antigen retrieval was achieved by boiling the tissue in 0.01 mol/L sodium citrate (pH 6.0) for 10 minutes. All of the primary antibodies were incubated overnight at 4°C. The protein was visualized by the brown pigmentation produced using the standard 3,3′-diaminobenzidine protocol. All sections were counterstained with hematoxylin to visualize nuclei and tissue structure.

Reverse transcription-PCR and quantitative reverse transcription-PCR analyses. Total RNA was extracted from cultured cells and from frozen gastric tissue specimens using ISOGEN reagent (NipponGene, Tokyo, Japan). The extracted RNA was treated with DNase I (Roche) and purified using the RNeasy MinElute Cleanup kit (Qiagen, Tokyo, Japan). The purified RNA was reverse transcribed and amplified by RT-PCR using the ImProm-II Reverse Transcription system (Promega, Madison, WI). The amplifications were done by denaturation at 95°C for 5 minutes, followed by 32 cycles of 60 seconds each at 95°C, 60°C, and 72°C. The following primer pairs were used: glyceraldehyde-3-phosphate dehydrogenase (GAPDH), 5′-GACATCAAGAAGGTGGTGAA-3′ and 5′-TGTCATACCAGGAAATGAGC-3′; Gli1, 5′-TGCCTTGTACCCTCCTCCCGAA-3′ and 5′-GCGATCTGTGATGGATGAGATTCCC-3′; Shh, 5′-ATGCTGCTGCTGGCGAGATGTCTGCTGCTA-3′ and 5′-TCAGCTGGACTTGACCGCCATGCCCAGCGG-3′; Smo, 5′-CTTCAGCTGCCACTTCTACGACTT-3′ and 5′-ACAGAAATATCCTGGGGCAGTATGG-3′; and Ptch, 5′-TTCTCACAACCCTCGGAACCCA-3′ and 5′-CTGCAGCTCAATGACTTCCACCTTC-3′.

The quantitative RT-PCR analysis was done also with a PCR mixture containing 1 μmol/L of each primer and SYBR Green master mix (Applied Biosystems, Foster City, CA). The amplifications were conducted at 95°C for 10 seconds and 60°C for 60 seconds using the ABI PRISM 7000 Quantitative PCR system (Applied Biosystems; ref. 32). Each sample was examined in triplicate and the amounts of the PCR products produced were normalized with respect to the GAPDH internal control. The following primer pairs were used: GAPDH, 5′-TGGGATTTCCATTGATGACAAG-3′ and 5′-CCACCCATGGCAAATTCC-3′; Gli1, 5′-GGCTGGACCAGCTACATCAAC-3′ and 5′-TGGTACCGGTGTGGGACAA-3′; p21/CIP1, 5′-CAGGGGACAGCAGAGGAAGA-3′ and 5′-TTAGGGCTTCCTCTTGGAGAA-3′; Ptch, 5′-CCACAGAAAACCCCGTCTTC-3′ and 5′-GGTTCGAGGGTGGGTGATG-3′; and Shh, 5′-GAGCGGACAGGCTGATGACT-3′ and 5′-CCTGGCCACTGGTTCATCAC-3′.

Analysis of gene expression using cDNA array assays. AGS cells were seeded onto 10-cm dishes, transfected with the siGli1 or control plasmid, and then cultured with puromycin for 24 hours. Seventy-two hours after transfection, the total RNA was extracted and used for cDNA array analysis as previously described (33). The cDNA array membranes contained 96 genes that are closely related to the cell cycle (Human Cell Cycle Gene Array, SuperArray Bioscience, Frederick, MD).

Cell proliferation assay. The cells were seeded onto six-well plates at a density of 2×10^4 cells per well. Cyclopamine dissolved in DMSO or DMSO alone was added to some wells at 0 hours. The number of viable cells was determined in triplicate wells at 24, 48, and 72 hours using the 3-(4,5-dimethylthiazol-2-yl)-2,5-diphenyltetrazolium bromide (MTT) assay (Sigma-Aldrich; refs. 34, 35).

Reporter assay. The p53 reporter assay was done using AGS and MKN1 cells as previously described (27). Briefly, 1×10^5 cells were plated onto a six-well tissue culture plate 24 hours before transfection. The transfection complexes containing a total of 0.6 μg of plasmid DNA (0.29 μg of the p53 reporter plasmid, 0.01 μg of pRL-TK, and a total of 0.3 μg of the p53 and Gli1 expression plasmids or the empty plasmids) and the FuGene transfection reagent were then added to each well. Cyclopamine dissolved in DMSO or DMSO alone was added 24 hours after transfection. The cells were harvested 48 hours after transfection and luciferase assays were carried out using the PicaGene Dual Sea Pansy system (Toyo Ink). The firefly and sea pansy luciferase activities were measured as relative light units with a luminometer (Lumat LB9507, EG&G Berthold, Bad Wildbad, Germany). The firefly luciferase activity was normalized to that of the sea pansy luciferase to control for transfection efficiency. All assays were done at least in triplicate.

Cell cycle analysis. AGS cells were seeded onto 10-cm dishes and were cultured for 72 hours under the conditions indicated in the text. The cells were harvested by trypsinization, fixed with 70% ethanol, and stained with propidium iodide before analysis of the DNA content by flow cytometry (36). The cell cycle phases were analyzed using MultiCycle software (Beckman Coulter, Fullerton, CA).

Statistics. The results are presented as mean ± SE. Comparisons were made using two-tailed Student's t test. $P < 0.05$ was considered statistically significant.

Results

The Sonic hedgehog ligand is constitutively expressed and has an essential role in the proliferation of gastric carcinoma cells cultured *in vitro*. The expression of Shh ligand mRNA was detected by RT-PCR in all five gastric carcinoma cell lines examined, as was the expression of Ptch, Smo, and Gli1 (Fig. 1*A*). The expression of Shh protein was also confirmed in all five gastric carcinoma cell lines but not in HEK 293T cells derived from embryonic kidneys (Fig. 1*B*). By contrast, the expression of Indian hedgehog protein was barely detectable in gastric carcinoma cells (data not shown). Treatment of AGS cells with anti-Shh blocking antibody inhibited cell proliferation in a dose-dependent manner as did treatment with cyclopamine, a specific inhibitor of Smo, as previously reported (17); conversely, the overexpression of Gli1 accelerated AGS cell growth (Fig. 1*C*). The quantitative RT-PCR analysis showed that the anti-Shh blocking antibody reduced the

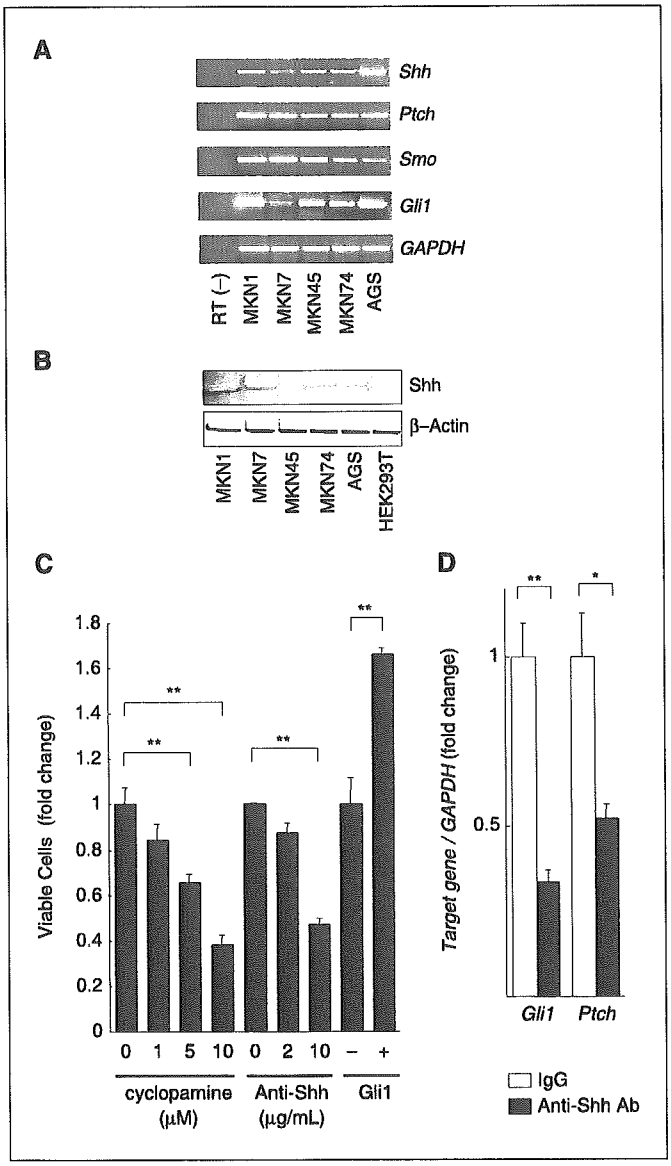

Figure 1. Constitutive expression of Shh induces cell proliferation in gastric carcinoma cell lines. *A*, RT-PCR analysis of the expressions of major molecules involved in Hh signaling, Shh, Ptch, Smo, and Gli1, in the five gastric carcinoma cell lines. *GAPDH* gene expression served as an internal control. Control, samples of total RNA from gastric carcinoma cells without reverse transcription reaction. *B*, immunoblot of Shh expression in the five gastric carcinoma cell lines. *C*, effects of treatment with anti-Shh blocking antibody or cyclopamine on the proliferation of AGS cells transfected with either a Gli1 expression vector or empty vector as determined by MTT assays at 72 hours after seeding. Results of MTT assays were independently normalized to the appropriate DMSO, IgG, or empty vector controls. *Columns*, mean fold changes relative to the control from three independent experiments; *bars*, SE. *D*, quantification of Ptch and Gli1 gene expressions in AGS cells with Hh antibody treatment using quantitative RT-PCR. *Columns*, mean of three experiments; *bars*, SE. *, $P < 0.05$; **, $P < 0.01$.

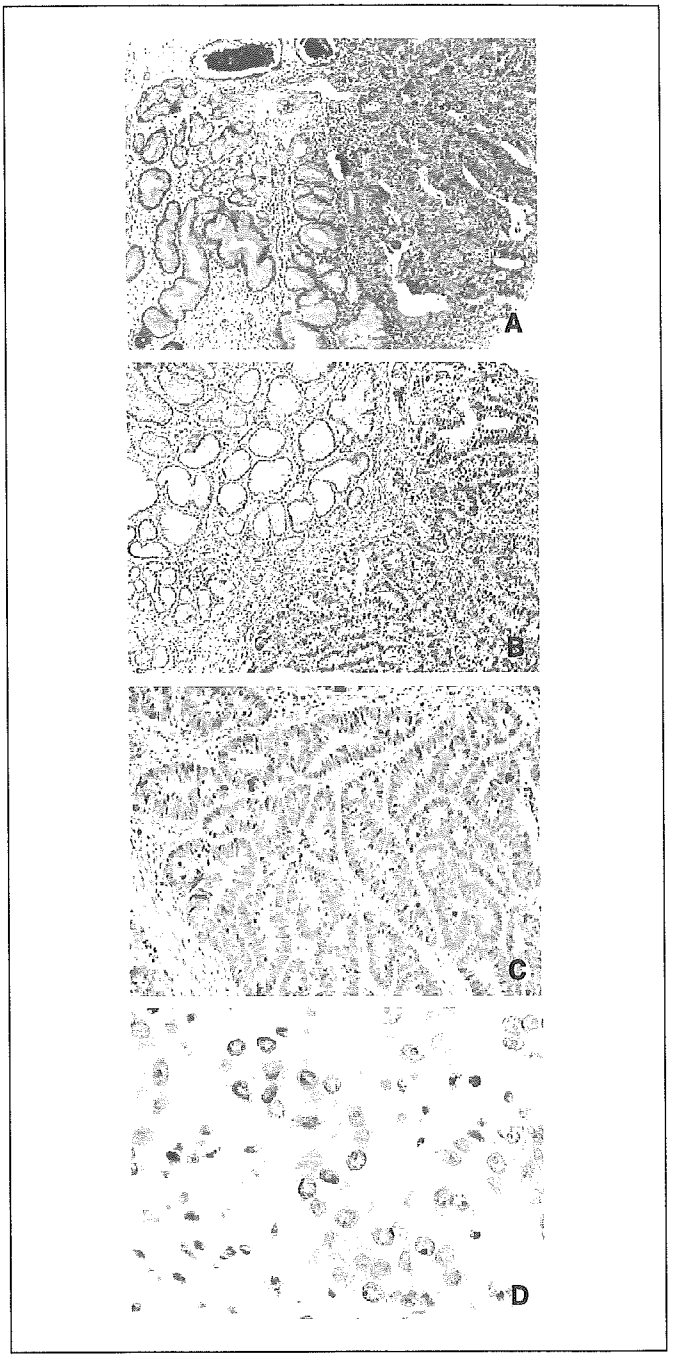

Figure 2. Expressions of Shh and Gli1 in gastric carcinoma tissues. Representative H&E staining (*A*) and expressions of Shh (*B* and *C*) and Gli1 (*D*) in gastric cancer tissues. *A* and *B*, *right*, cancer tissue; *left*, noncancerous tissue. The Shh ligand was expressed mainly in the cytoplasm (*C*) and Gli1 was strongly expressed in both the cytoplasm and nuclei (*D*) of gastric carcinoma cells. All sections were counterstained with hematoxylin to visualize nuclei and tissue structure. Magnifications: ×40 (*A*, *B*), ×100 (*C*), and ×200 (*D*).

expression of Gli1 and Ptch (Fig. 1*D*), both of which are well-known target genes regulated by Hh signaling (18). We also confirmed that the Shh blocking antibody did not affect the growth of HEK 293T embryonic kidney cells (data not shown), which did not express Shh. These findings suggest that the Shh-Smo-Gli1 pathway has a pivotal role in the growth of gastric cancer cells and that stimulation of Hh signaling by Shh ligand occurs in an autocrine/paracrine manner in gastric cancer cells.

Sonic hedgehog is overexpressed in human gastric carcinoma tissues. To analyze the expression of Shh ligand in normal and gastric carcinoma tumor tissues collected from patients who had undergone gastrectomy, sections of cancerous or noncancerous tissues were stained by immunohistochemistry using anti-Shh antibody. Compared with the expression level in normal tissues, Shh was constitutively overexpressed in gastric tumors (Fig. 2*B* and *C*). Gli1 was up-regulated and imported into the nucleus by activated Hh signaling (20, 37–39); we detected high levels of Gli1 in the nuclei of gastric carcinoma cells, as well as in the cytoplasm (Fig. 2*D*), suggesting that activated Hh signaling occurs in these tumors. The quantitative RT-PCR analysis of Shh mRNA expression revealed that Shh was overexpressed 12.8-fold (range, 0.3- to 78.8-fold) in 57% of gastric carcinoma tissues as compared with the expression level in the surrounding noncancerous gastric tissue (Table 1). There was no correlation between the level of Shh mRNA expression and the pathologic or clinical features of the tumor, including tumor type, size, location, and stage.

Decreased glioma-associated oncogene 1 expression by RNA interference inhibits the growth of gastric carcinoma cells. Gli1, a downstream transcriptional factor of Shh signal, is commonly expressed in gastric carcinoma cells and tumor tissues. To elucidate whether Gli1 is involved in the proliferation of cancer cells downstream from the Hh pathway, Gli1 was stably knocked down in cultured AGS cells using a Gli1-knockdown vector (siGli1). The reduction of endogenous Gli1 expression in AGS cells was confirmed by RT-PCR and immunoblot assays (Fig. 3*A* and *B*). The proliferation assay revealed that Gli1 knockdown markedly repressed AGS cell growth (41.0 ± 8.0% after 72 hours; Fig. 3*D*). Moreover, Gli1 knockdown led to a significant increase in the proportion of cells in G_1 phase (58.2 ± 1.1% versus 43.2 ± 0.9%, $P < 0.01$; Fig. 3*E*) and a significant decrease in the proportion of cells in S phase (14.4 ± 1.6% versus 30.9 ± 1.6%, $P < 0.01$) as compared with the control AGS cells. Similar results were found when AGS cells transfected with the empty vector were used as the negative control (data not shown). For further confirmation that this growth suppression effect of Gli1 knockdown is attributable to the blockade of Hh signaling, the growth rate under the coexpression of siGli1 and active Smo-W539L was also examined in AGS cells. The MTT assay showed that active Smo expression did not antagonize the tumor growth suppression caused by Gli1 knockdown (Fig. 3*D*). This result indicates that the growth effect gained by activated Hh signaling is mainly through the Gli1 protein. These findings suggest that Gli1 plays a pivotal role in cell proliferation through regulation of the G_1-S transition and that Gli1 is implicated in the Shh-dependent autocrine loop that accelerates the proliferation of gastric carcinoma cells.

Glioma-associated oncogene 1 knockdown induces an increase in p21/cyclin-dependent kinase–interacting protein 1 expression in gastric carcinoma cells. To unravel the details of the molecular systems that are regulated by Hh-Gli1 signaling and that contribute to cell proliferation in gastric carcinoma cells, we used a cell cycle gene cDNA array to examine the expression profile of genes involved in the difference in the cell cycle of AGS cells transfected with the siGli1 or siGFP control vector. We noted that the expression of p21/CIP1 mRNA was up-regulated in cells in which Gli1 expression was decreased whereas the expression levels of other CDK inhibitors were not significantly different (Fig. 4*A*). Analysis using quantitative RT-PCR and immunoblot assays confirmed that p21/CIP1 expression

Table 1. Clinical features of 14 patients with gastric carcinoma and levels of Shh mRNA expression in the lesions compared with the levels in noncancerous tissues

Patient no.	Age/sex	Differentiation*	Vascular invasion	Tumor-node-metastasis classification	Location†	Tumor size (cm)	Shh expression‡
1	48/M	Mod	–	$T_3N_1M_0$	C	4 × 3	5.2
2	70/M	Por	–	$T_3N_0M_0$	A	3 × 2	6.2
3	69/M	Pap	+	$T_2N_0M_0$	B	6 × 5	8.2
4	70/M	Muc	–	$T_1N_1M_0$	B	3 × 3	24.2
5	69/F	Muc	–	$T_2N_0M_0$	B	5 × 5	1.7
6	42/M	Sig	–	$T_1N_0M_0$	B	2 × 2	0.3
7	60/M	Por	+	$T_3N_1M_0$	B, A	8 × 7	1.1
8	69/M	Por	+	$T_1N_0M_0$	C	5 × 5	10.0
9	54/M	Por	+	$T_2N_0M_0$	B	4 × 4	78.7
10	81/M	Mod	–	$T_1N_0M_0$	C	4 × 3	17.1
11	74/F	Mod	–	$T_1N_0M_0$	B	3 × 3	19.5
12	55/M	Mod	+	$T_2N_0M_0$	B	5 × 5	1.8
13	48/M	Sig	+	$T_3N_1M_0$	B, A	15 × 13	0.6
14	68/M	Mod	+	$T_2N_1M_0$	A	7 × 6	0.4

*Mod, moderately differentiated; Muc, mucinous; Pap, papillary; Por, poorly differentiated; Sig, signet ring.
†Location: C, cardia; B, body; A, antrum.
‡Relative expression ratio of the level of Shh mRNA in the cancerous lesion compared with the level in the surrounding noncancerous tissue as determined by quantitative RT-PCR analysis.

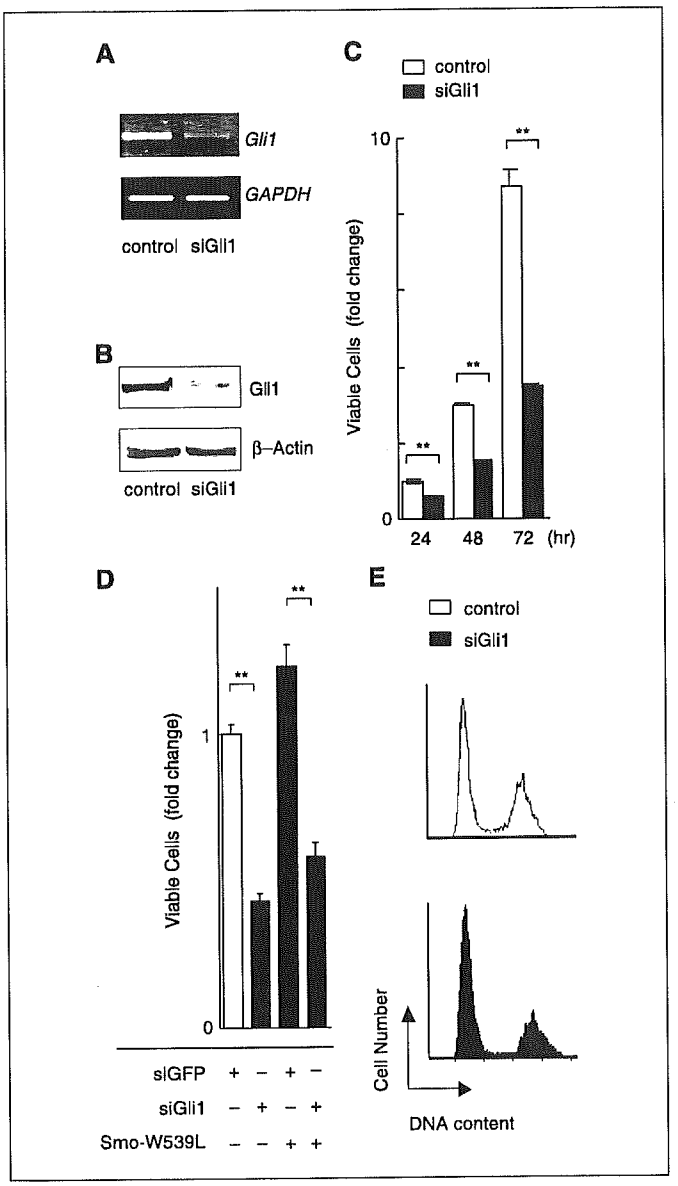

Figure 3. Suppression of AGS cell growth induced by Gli1 knockdown. Gli1 expression 72 hours after transfection with the siGli1 vector analyzed by RT-PCR (*A*) and immunoblotting (*B*). Proliferation of AGS cells by siGli1 transfection (24, 48, and 72 hours after reseeding; *C*) and by cotransfection with active Smo expression vector (Smo-W539L) and siGli1 (48 hours after reseeding; *D*). *Columns*, mean fold changes relative to the control from three independent experiments; *bars*, SE. **, $P < 0.01$. *E*, AGS cells were transfected with the siGli1 or control siGFP vector, harvested after 72 hours, stained with propidium iodide, and analyzed by flow cytometry. Representative data from one of three independent experiments.

was up-regulated at both the mRNA and protein levels by the knockdown of Gli1 in AGS cells (Fig. 4*B* and *C*). The inhibition of Hh signaling by cyclopamine treatment similarly increased p21/CIP1 expression and the transfection with Gli1 expression vector suppressed the cyclopamine-induced increase in p21/CIP1 (Fig. 4*D*). By contrast, the knockdown of Gli1 did not alter p27/KIP1 expression (Fig. 4*C* and *D*) and p16/INK4a and p19/INK4d could not be detected in AGS cells (data not shown). These results suggest that the negative regulation of p21/CIP1 expression by activated Hh signaling through Gli1 promotes growth in gastric carcinoma cells.

The up-regulation of p21/cyclin-dependent kinase–interacting protein 1 and the cell cycle arrest induced by the blockade of Hedgehog signaling are p53 independent. The tumor suppressor p53 is a major transcription factor involved in the regulation of p21/CIP1 expression. We examined the contribution of p53 to the observed up-regulation of p21/CIP1 by the blockade of Hh signaling in gastric carcinoma cells. Both AGS cells and MKN45 cells express wild-type p53 (40, 41) whereas MKN1 and MKN74 cells express mutated p53 proteins (V143A substitution in MKN1 and I251L and E271A substitutions in MKN74; ref. 41). Although the inhibition of Hh signaling by cyclopamine treatment induced an increase in both p21/CIP1 mRNA (Fig. 5*A*) and protein (Fig. 5*B*) in AGS, MKN1, MKN45, and MKN74 cells, it did not affect the expression of p53 in these cell lines (Fig. 5*B*). In addition, the luciferase activity in AGS and MKN1 cells transfected with a luciferase reporter plasmid containing the p53 response element was not affected by cotransfection with a Gli1 expression vector or by cyclopamine

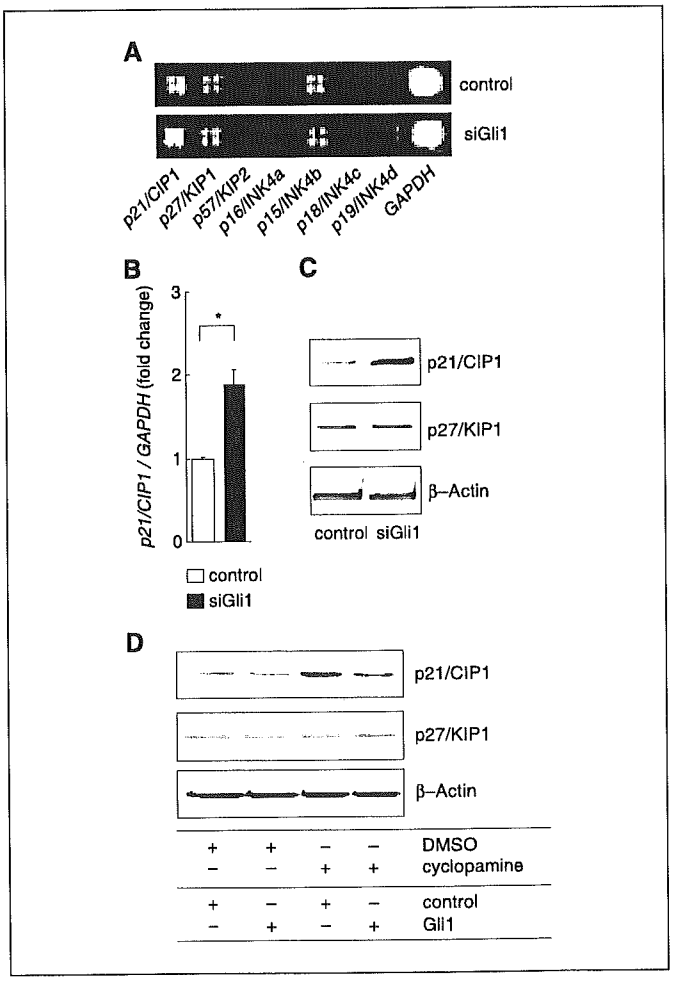

Figure 4. Expression of p21/CIP1 was negatively regulated by Hh-Gli1 signaling in AGS cells. *A*, AGS cells were transfected with the siGli1 or control siGFP vector 72 hours before total RNA extraction and cDNA array analysis. *B*, p21/CIP1 gene expression level was confirmed by quantitative RT-PCR analysis. *Columns*, mean of three experiments; *bars*, SE. *, $P < 0.02$. *C*, expression levels of p21/CIP1 and p27/KIP1 examined by immunoblot assay. *D*, AGS cells were transfected with Gli1 expression vector or empty vector 24 hours before treatment with cyclopamine (10 μmol/L). Levels of p21/CIP1 and p27/KIP1 expressions were examined 72 hours after transfection.

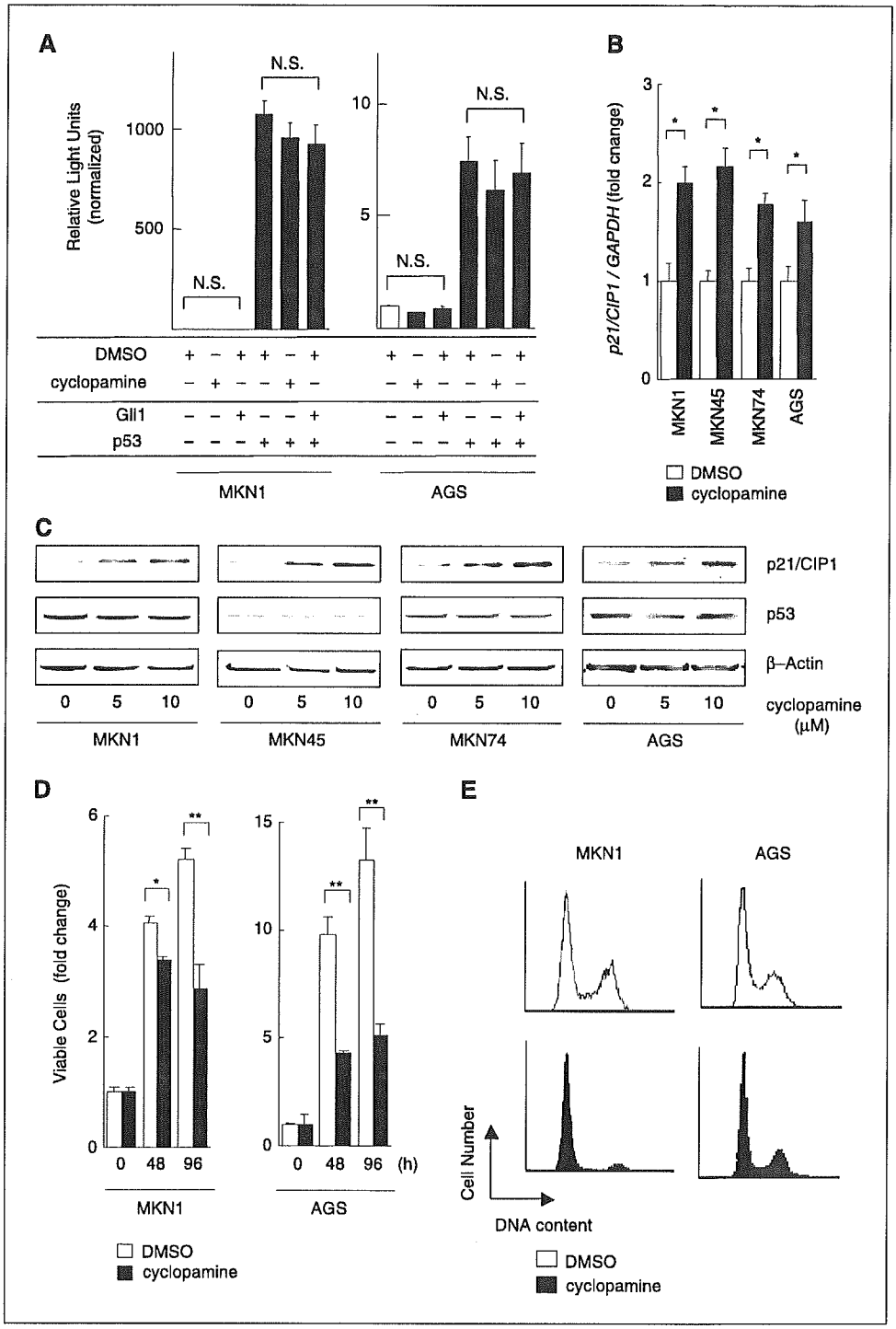

Figure 5. Up-regulation of p21/CIP1 expression by the blockade of Hh signaling was independent of p53 status. *A*, expression of p21/CIP1 analyzed using quantitative RT-PCR 24 hours after treatment with cyclopamine (10 μmol/L) or DMSO alone. *B*, effects of the inhibition of Hh signaling by cyclopamine treatment on the expression levels of p21/CIP1 and p53 proteins in AGS, MKN1, MKN45, and MKN74 cells 24 hours after cyclopamine treatment. *C*, AGS and MKN1 cells were transfected with the p53 reporter plasmid expressing firefly luciferase, together with the Gli1 and/or p53 expression vectors, as well as the *Renilla* luciferase vector, 24 hours before treatment with cyclopamine (10 μmol/L) or DMSO alone for 24 hours. Forty-eight hours after transfection, the cells were harvested and the amount of luciferase activity was measured and normalized to the *Renilla* luciferase activity. *D*, proliferation of AGS and MKN1 cells 48 and 96 hours after treatment with cyclopamine (10 μmol/L) or DMSO. Results of MTT assay reported as fold changes relative to the 0 hours control. *E*, AGS and MKN1 cells were treated with cyclopamine (10 μmol/L) or DMSO alone, harvested after 72 hours, stained with propidium iodide, and analyzed by flow cytometry. Results from three experiments. *, $P < 0.05$; **, $P < 0.02$.

treatment (Fig. 5*C*). The inhibitory effect of cyclopamine treatment on cell growth was observed in MKN1 cells as well as in AGS cells (Fig. 5*D*). Cell cycle analysis showed that the blockade of Hh signaling in AGS cells by cyclopamine treatment increased the proportion of cells in G_1 phase (54.3 ± 0.2% versus 45.4 ± 0.8%, $P < 0.03$) and decreased the proportion of cells in S phase (24.3 ± 0.8% versus 37.2 ± 0.8%, $P < 0.01$; Fig. 5*E*). Similarly, the proportions of MKN1 cells in G_1 and S phase were increased (78.5 ± 0.1% versus 38.6 ± 0.4%, $P < 0.01$) and decreased (13.0 ± 0.1% versus 34.2 ± 0.2%, $P < 0.01$), respectively (Fig. 5*E*). These results suggest that the increased expression of p21/CIP1 and the inhibition of the G_1-S cell cycle transition are induced in a p53-independent manner by the blockade of Hh signaling in gastric carcinoma cells.

Discussion

Although some recent studies have indicated that Hh signaling is constitutively activated in gastric carcinoma cells (17, 23), the cancer-specific mechanism of this constitutive activation remains

unclear. Treatment with the Smo inhibitor has been reported to be effective for various cancers; however, the molecules involved in the cyclopamine-induced inhibition of cancer cell growth are also unknown. This study showed that gastric carcinoma cells constitutively produced the Shh ligand, thereby activating downstream signaling both *in vitro* and *in vivo*, and that Shh-Gli1 signaling negatively regulated the expression of the CDK inhibitor p21/CIP1 in gastric carcinoma cells.

Several growth signals mediate the accelerated growth of cancer cells by autocrine loops involving the expressions of both ligand and receptor by the same cell. The Shh ligand was constitutively expressed in all of the cultured gastric carcinoma cell lines we examined; the growth of these cells was inhibited by anti-Shh blocking antibody as well as by cyclopamine. Moreover, the overexpression of Shh in gastric carcinoma cells was also confirmed in many specimens of human gastric carcinoma tissues collected at gastrectomy. The overexpression of Shh ligand and the resulting autocrine/paracrine loop might partly explain the abnormal activation of the Hh pathway in gastric carcinoma cells. We found no specific correlation between the constitutive expression of Shh in gastric carcinomas and their clinical characteristics; consequently, Hh signaling might be one of the growth regulatory mechanisms involved in the initial stages of malignant cell transformation. To determine the contribution of abnormal Hh signaling to carcinogenesis, it is crucial to examine whether Hh signaling is activated in benign tumors and early-stage cancers, as well as in progressing tumors.

The results suggest that the oncogene Gli1 also has a pivotal role in the proliferation of gastric carcinoma cells. Strikingly, the cDNA arrays showed that the disruption of Gli1 expression by small interfering RNA increased the expression of p21/CIP1 mRNA and protein. p21/CIP1 can induce G_1 arrest and block S-phase entry by inactivating CDKs (42) and the overexpression of p21/CIP1 effectively suppresses tumor growth (43). In addition, defects in p21/CIP1 increase susceptibility to chemically induced carcinoma formation (44). These findings imply that Shh-Gli1 signaling accelerates the G_1-S transition by down-regulating the expression of p21/CIP1, thereby inducing increased proliferation of gastric carcinoma cells.

The regulation of p21/CIP1 by Hh signaling in gastric carcinoma cells was independent of p53. Although the p53 protein is one of the most important transcriptional factors regulating p21/CIP1 expression (45, 46), Hh signaling did not affect the expression or activity of p53 and the inhibition of Hh signaling increased p21/CIP1 expression even in gastric carcinoma cells with mutated *p53* genes. It is possible that Hh signaling pathways cross talk with other signaling pathways, such as those involving MYC, SMAD, and FOX regulatory and transcription factors (46–48), which repress the expression of p21/CIP1 in a p53-independent manner in tumor cells. The relationship between abnormal Hh signaling and change-of-function mutations in other genes in gastric cancer should also be examined.

In conclusion, this study showed that Hh signaling may control cell proliferation through the negative regulation of p21/CIP1 expression in gastric carcinoma cells. Although many details of the molecular biology of Hh signaling in the digestive tract remain to be elucidated, a deeper understanding of these pathways may shed light on the mechanisms of carcinogenesis in gastric tumors and may lead to the development of novel therapeutic strategies for gastric carcinomas in the near future.

Acknowledgments

Received 3/6/2005; revised 7/19/2005; accepted 8/12/2005.

The costs of publication of this article were defrayed in part by the payment of page charges. This article must therefore be hereby marked *advertisement* in accordance with 18 U.S.C. Section 1734 solely to indicate this fact.

We thank Mitsuko Tsubouchi, Sanae Ogawa, and the members of the Sata laboratory for their technical assistance; and Drs. T. Motojima and S. Yamada (Division of Abdominal Surgery, Motojima General Hospital, Gumma, Japan), Dr. T. Oyama (Division of Pathology, Motojima General Hospital), Dr. H. Sasaki (RIKEN Center for Developmental Biology, Kobe, Japan), Dr. P.A. Beachy (Department of Oncology, Johns Hopkins University School of Medicine, Baltimore, MD), Drs. B. Vogelstein and K.W. Kinzler (Howard Hughes Medical Institute, Sidney Kimmel Comprehensive Cancer Center and Program in Human Genetics and Molecular Biology, Johns Hopkins Medical Institutions, Baltimore, MD), and the Developmental Studies Hybridoma Bank for supplying key materials.

References

1. Ingham PW, McMahon AP. Hedgehog signaling in animal development: paradigms and principles. Genes Dev 2001;15:3059–87.
2. Lum L, Beachy PA. The Hedgehog response network: sensors, switches, and routers. Science 2004;304:1755–9.
3. Huang Z, Kunes S. Hedgehog, transmitted along retinal axons, triggers neurogenesis in the developing visual centers of the *Drosophila* brain. Cell 1996;86:411–22.
4. Wang B, Fallon JF, Beachy PA. Hedgehog-regulated processing of Gli3 produces an anterior/posterior repressor gradient in the developing vertebrate limb. Cell 2000;100:423–34.
5. Ramalho-Santos M, Melton DA, McMahon AP. Hedgehog signals regulate multiple aspects of gastrointestinal development. Development 2000;127:2763–72.
6. Zhang Y, Kalderon D. Hedgehog acts as a somatic stem cell factor in the *Drosophila* ovary. Nature 2001; 410:599–604.
7. Machold R, Hayashi S, Rutlin M, et al. Sonic hedgehog is required for progenitor cell maintenance in telencephalic stem cell niches. Neuron 2003;39:937–50.
8. Taipale J, Beachy PA. The Hedgehog and Wnt signalling pathways in cancer. Nature 2001;411:349–54.
9. Pasca di Magliano M, Hebrok M. Hedgehog signalling in cancer formation and maintenance. Nat Rev Cancer 2003;3:903–11.
10. Hahn H, Wicking C, Zaphiropoulous PG, et al. Mutations of the human homolog of *Drosophila* patched in the nevoid basal cell carcinoma syndrome. Cell 1996; 85:841–51.
11. Johnson RL, Rothman AL, Xie J, et al. Human homolog of patched, a candidate gene for the basal cell nevus syndrome. Science 1996;272:1668–71.
12. Dahmane N, Lee J, Robins P, Heller P, Ruiz i Altaba A. Activation of the transcription factor Gli1 and the Sonic hedgehog signalling pathway in skin tumours. Nature 1997;389:876–81.
13. Berman DM, Karhadkar SS, Hallahan AR, et al. Medulloblastoma growth inhibition by hedgehog pathway blockade. Science 2002;297:1559–61.
14. Dahmane N, Sanchez P, Gitton Y, et al. The Sonic Hedgehog-Gli pathway regulates dorsal brain growth and tumorigenesis. Development 2001;128:5201–12.
15. Watkins DN, Berman DM, Burkholder SG, Wang B, Beachy PA, Baylin SB. Hedgehog signalling within airway epithelial progenitors and in small-cell lung cancer. Nature 2003;422:313–7.
16. Thayer SP, di Magliano MP, Heiser PW, et al. Hedgehog is an early and late mediator of pancreatic cancer tumorigenesis. Nature 2003;425:851–6.
17. Berman DM, Karhadkar SS, Maitra A, et al. Widespread requirement for Hedgehog ligand stimulation in growth of digestive tract tumours. Nature 2003; 425:846–51.
18. Sanchez P, Hernandez AM, Stecca B, et al. Inhibition of prostate cancer proliferation by interference with Sonic Hedgehog-GLI1 signaling. Proc Natl Acad Sci U S A 2004;101:12561–6.
19. Karhadkar SS, Steven Bova G, Abdallah N, et al. Hedgehog signalling in prostate regeneration, neoplasia and metastasis. Nature 2004;431:707–12.
20. Kubo M, Nakamura M, Tasaki A, et al. Hedgehog signaling pathway is a new therapeutic target for patients with breast cancer. Cancer Res 2004;64:6071–4.
21. Xie J, Murone M, Luoh SM, et al. Activating Smoothened mutations in sporadic basal-cell carcinoma. Nature 1998;391:90–2.
22. Unden AB, Holmberg E, Lundh-Rozell B, et al. Mutations in the human homologue of *Drosophila* patched (PTCH) in basal cell carcinomas and the Gorlin syndrome: different *in vivo* mechanisms of PTCH inactivation. Cancer Res 1996;56:4562–5.
23. Ma X, Chen K, Huang S, et al. Frequent activation of the hedgehog pathway in advanced gastric adenocarcinomas. Carcinogenesis 2005;26:1698–705.
24. Taipale J, Cooper MK, Maiti T, Beachy PA. Patched acts catalytically to suppress the activity of Smoothened. Nature 2002;418:892–7.
25. Kinzler KW, Ruppert JM, Bigner SH, Vogelstein B. The GLI gene is a member of the Kruppel family of zinc finger proteins. Nature 1988;332:371–4.
26. Sasaki H, Hui C, Nakafuku M, Kondoh H. A binding

site for Gli proteins is essential for HNF-3β floor plate enhancer activity in transgenics and can respond to Shh *in vitro*. Development 1997;124:1313–22.
27. Otsuka M, Kato N, Lan K, et al. Hepatitis C virus core protein enhances p53 function through augmentation of DNA binding affinity and transcriptional ability. J Biol Chem 2000;275:34122–30.
28. Taipale J, Chen JK, Cooper MK, et al. Effects of oncogenic mutations in Smoothened and Patched can be reversed by cyclopamine. Nature 2000;406:1005–9.
29. Miyagishi M, Taira K. U6 promoter-driven siRNAs with four uridine 3′ overhangs efficiently suppress targeted gene expression in mammalian cells. Nat Biotechnol 2002;20:497–500.
30. Jazag A, Ijichi H, Kanai F, et al. Smad4 silencing in pancreatic cancer cell lines using stable RNA interference and gene expression profiles induced by transforming growth factor-β. Oncogene 2004;24:662–71.
31. Kanai F, Marignani PA, Sarbassova D, et al. TAZ: a novel transcriptional co-activator regulated by interactions with 14-3-3 and PDZ domain proteins. EMBO J 2000;19:6778–91.
32. Ijichi H, Otsuka M, Tateishi K, et al. Smad4-independent regulation of p21/WAF1 by transforming growth factor-β. Oncogene 2004;23:1043–51.
33. Yanai A, Hirata Y, Mitsuno Y, et al. Helicobacter pylori induces antiapoptosis through nuclear factor-κB activation. J Infect Dis 2003;188:1741–51.
34. Otsuka M, Kato N, Shao RX, et al. Vitamin K2 inhibits the growth and invasiveness of hepatocellular carcinoma cells via protein kinase A activation. Hepatology 2004;40:243–51.
35. Kanai F, Kawakami T, Hamada H, et al. Adenovirus-mediated transduction of Escherichia coli uracil phosphoribosyltransferase gene sensitizes cancer cells to low concentrations of 5-fluorouracil. Cancer Res 1998;58:1946–51.
36. Sata M, Perlman H, Muruve DA, et al. Fas ligand gene transfer to the vessel wall inhibits neointima formation and overrides the adenovirus-mediated T cell response. Proc Natl Acad Sci U S A 1998;95:1213–7.
37. Kogerman P, Grimm T, Kogerman L, et al. Mammalian suppressor-of-fused modulates nuclear-cytoplasmic shuttling of Gli-1. Nat Cell Biol 1999;1:312–9.
38. Dai P, Akimaru H, Tanaka Y, Maekawa T, Nakafuku M, Ishii S. Sonic Hedgehog-induced activation of the Gli1 promoter is mediated by GLI3. J Biol Chem 1999;274:8143–52.
39. Barnes EA, Heidtman KJ, Donoghue DJ. Constitutive activation of the shh-ptc1 pathway by a patched1 mutation identified in BCC. Oncogene 2005;24:902–15.
40. Jiang XH, Wong BC, Lin MC, et al. Functional p53 is required for triptolide-induced apoptosis and AP-1 and nuclear factor-κB activation in gastric cancer cells. Oncogene 2001;20:8009–18.
41. Ohashi M, Kanai F, Ueno H, et al. Adenovirus mediated p53 tumour suppressor gene therapy for human gastric cancer cells *in vitro* and *in vivo*. Gut 1999;44:366–71.
42. Gartel AL, Serfas MS, Tyner AL. p21-negative regulator of the cell cycle. Proc Soc Exp Biol Med 1996;213:138–49.
43. Hsiao M, Tse V, Carmel J, et al. Functional expression of human p21(WAF1/CIP1) gene in rat glioma cells suppresses tumor growth *in vivo* and induces radiosensitivity. Biochem Biophys Res Commun 1997;233:329–35.
44. Topley GI, Okuyama R, Gonzales JG, Conti C, Dotto GP. p21(WAF1/Cip1) functions as a suppressor of malignant skin tumor formation and a determinant of keratinocyte stem-cell potential. Proc Natl Acad Sci U S A 1999;96:9089–94.
45. el-Deiry WS, Tokino T, Velculescu VE, et al. WAF1, a potential mediator of p53 tumor suppression. Cell 1993;75:817–25.
46. Massague J. G_1 cell-cycle control and cancer. Nature 2004;432:298–306.
47. van de Wetering M, Sancho E, Verweij C, et al. The β-catenin/TCF-4 complex imposes a crypt progenitor phenotype on colorectal cancer cells. Cell 2002;111:241–50.
48. Seoane J, Le HV, Shen L, Anderson SA, Massague J. Integration of Smad and forkhead pathways in the control of neuroepithelial and glioblastoma cell proliferation. Cell 2004;117:211–23.

RESEARCH ARTICLE

Profound Cardiac Sympathetic Denervation Occurs in Parkinson Disease

Takeshi Amino[1,2,5]; Satoshi Orimo[1,2]; Yoshinori Itoh[3]; Atsushi Takahashi[4]; Toshiki Uchihara[2]; Hidehiro Mizusawa[5]

[1] Department of Neurology, Kanto Central Hospital, Tokyo, Japan.
[2] Department of Neuropathology, Tokyo Metropolitan Institute for Neuroscience, Japan.
[3] Department of Internal Medicine, [4]Department of Organ and Function Pathology, Yokufukai Geriatric Hospital, Tokyo, Japan.
[5] Department of Neurology and Neurological Science, Tokyo Medical and Dental University, Japan.

Corresponding author:
Satoshi Orimo, MD., Department of Neurology, Kanto Central Hospital, 6-25-1 Kami-Yoga, Setagaya-ku, 158-8531, Tokyo, Japan (E-mail: orimo@kanto-ctr-hsp.com)

In the last few years, cardiac sympathetic dysfunction in Parkinson disease (PD) has been postulated on the basis of decreased cardiac uptake of sympathoneural imaging tracers. However, the pathological substrate for the dysfunction remains to be established. We examined the left ventricular anterior wall from postmortem specimens with immunohistochemical staining for tyrosine hydroxylase (TH), neurofilament (NF) and S-100 protein in PD patients and control subjects, and quantified the immunoreactive areas. As TH-immunoreactive axons nearly disappeared and NF-immunoreactive axons drastically decreased in number, the morphological degeneration of the cardiac sympathetic nerves in PD was confirmed. Quantitative analysis showed that sympathetic nerves were preferentially involved. Triple immunofluorolabeling for NF, TH, and myelin basic protein showed clearly the profound involvement of sympathetic axons in PD. The extent of involvement of the cardiac sympathetic nerves seems likely to be equivalent to that in the central nervous system, including the nigrostriatal dopaminergic system. PD affects the cardiac sympathetic nervous system profoundly as well as nigrostriatal dopaminergic system.

Brain Pathol 2005;15:29-34.

INTRODUCTION

Parkinson disease (PD) is not only a disease of the nigrostriatal dopaminergic system but also a disease of the autonomic nervous system. Therefore, symptoms of autonomic dysfunction such as constipation, orthostatic and postprandial hypotension, dyshidrosis and bladder dysfunction occur commonly in PD (32).

Recent awareness of a decrease in cardiac uptake of [^{123}I]*meta*-iodobenzylguanidine (MIBG) on single photon emission computed tomography (SPECT) or of 6-[^{18}F]fluorodopamine (6F-DA) on positron emission tomography (PET) in PD patients is now attracting increasing attention because this decreased uptake is detectable before other autonomic disturbances are evident (6, 24, 39). Moreover, this decrease is of particular clinical importance because it is usually undetectable in patients with multiple system atrophy (MSA), progressive supranuclear palsy (PSP) (39) or corticobasal degeneration (CBD) (23) and could therefore be helpful in isolating PD from among the various parkinsonian syndromes.

The decreased cardiac uptake of these sympathoneural radiotracers may represent dysfunction of the cardiac sympathetic system in PD (6). Indeed, our recent immunohistochemical study demonstrated a marked decrease in tyrosine hydroxylase (TH)-immunoreactive+ axons in the epicardium of the left ventricular anterior wall in PD patients (22, 25). This pathological finding was considered to represent the involvement of the cardiac sympathetic nerves in PD and presumably accounts for the decreased cardiac uptake of the tracers. However, it remains to be clarified whether morphological depletion of the sympathetic nerves and denervation occurs or whether they are merely functionally involved, and whether TH+ axons are selectively affected.

In this case-control study, we observed neurofilament (NF)-immunoreactive axons coupled with TH+ axons, and quantified the frequency of TH+ axons relative to NF+ axons. In addition, we investigated their relation to myelin and Schwann cells. Triple immunofluorolabeling for NF, TH and myelin basic protein (MBP) demonstrated clearly the profound involvement of TH+ axons in PD patients.

MATERIALS AND METHODS

Subjects. Cardiac tissue samples obtained at autopsy from four PD patients and 5 control subjects were used in this study. Clinical diagnosis of PD was based on dopa-responsive parkinsonian symptoms (tremor, muscle rigidity, akinesia and postural instability). The postmortem examination revealed marked neuronal loss and numerous Lewy bodies in the substantia nigra, locus ceruleus and dorsal vagal nucleus. Five control subjects without parkinsonian symptoms and signs, primary heart disease, diabetes mellitus and peripheral neuropathy, were enrolled. The postmortem examinations confirmed the absence of Lewy bodies in the central nervous system. There was no statistical difference in age between the PD patients and control subjects. (Table 1)

Immunohistochemical staining. The heart tissue was fixed in formalin at autopsy within 48 hours after death. Specimens were obtained from the left ventricular anterior wall and embedded in paraffin. The left ventricular wall was considered preferable for this study because PET or SPECT studies in healthy subjects show uniformly high radioactivity there. Four-micrometer thick sections sliced axially were deparaffinized and stained with hematoxylin and eosin (H&E).

We used the following primary antibodies for immunohistochemical staining: anti-NF (SMI-31, mouse monoclonal, 1:10000 SMI, Baltimore, Md) as a marker

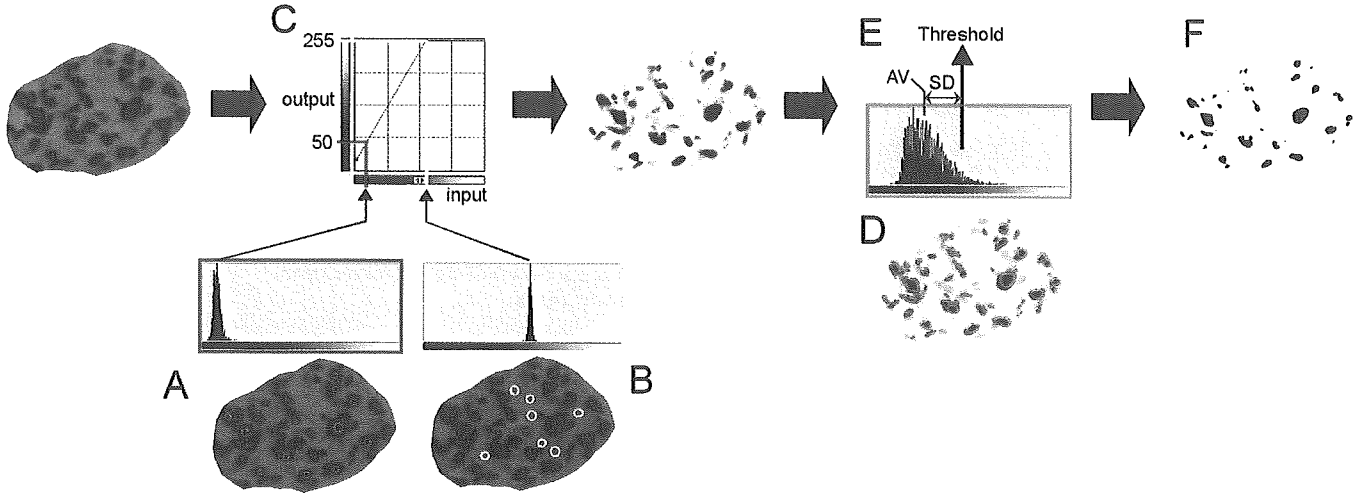

Figure 1. *Procedure for measuring immunoreactive areas.* **A.** On an 8-bit gray scale (0:black-255:white) image, several areas with the most intense immunoreactivity were circled and the mean value of these areas was calibrated to 50 on the 8-bit gray scale. **B.** In the same way, the mean value of several unstained areas was calibrated to 255. **C.** Based on these 2 calibration points, the entire image was transformed linearly into an 8-bit gray scale. **D.** On the transformed image, immunostained axonal areas were arbitrarily selected and their average value (AV) and standard deviation value (SD) were calculated. **E.** The entire image was then binarized with the threshold defined as the AV ± SD. **F.** Areas with a pixel value below the threshold were judged immunoreactive areas. Extracted areas were therefore considered reasonable as immunoreactive areas compared with the original digitalized image.

Case	Age at death	Gender	Duration of disease (years)	Hoehn and Yahr stage	Cause of death
PD 1	70	Male	10	5	Bronchitis
PD 2	82	Female	10	4	Colon cancer, ileus, sepsis
PD 3	83	Female	>3	5	Pneumonia
PD 4	91	Female	15	4	Pneumonia, chronic lymphocytic leukemia
Control 1	86	Female	-	-	Colon cancer
Control 2	89	Male	-	-	Esophageal cancer, pneumonia
Control 3	81	Female	-	-	Colon cancer, peritonitis
Control 4	93	Male	-	-	Acute respiratory failure, tracheitis
Control 5	91	Female	-	-	Acute respiratory failure, emphysema

Table 1. Characteristics of patients and control subjects.

for all axons, anti-TH (mouse monoclonal, 1:3000 SIGMA, Saint Louis, Mo) as a marker for catecholaminergic axons, anti-S-100 protein (mouse monoclonal, 1:1500 IBL, Gunma, Japan) as a marker for Schwann cells and anti-MBP (rabbit polyclonal, 1:1000 IBL) as a marker for myelin. An indirect immunofluorescence procedure using the avidin-biotin technique was employed. The deparaffinized sections were treated in a microwave oven with citrate buffer 3 times for 6 minutes, treated with 1% hydrogen peroxide for 30 minutes and then incubated with the primary antibody diluted with phosphate-buffered saline containing 0.03% Triton-X100 and the corresponding blocking serum. In order to reduce background stain and achieve optimal signal to noise ratio, we usually take 2 days or longer at 4°C for primary antibody incubation with higher dilution. The sections were then incubated for 2 hours with the biotinylated secondary antibody (anti-rabbit or anti-mouse, 1:1000, Vector, Burlingame, Calif), followed by avidin-biotin-peroxidase complex (1:1000 ABC Elite, Vector). The peroxidase labeling was visualized with diaminobenzidine-nickel as chromogen, and then the stained sections were lightly stained with fast nuclear red solution.

Quantification procedure. Relatively large (diameter >50 μm) and round (maximum diameter/minimum diameter <2) nerve fascicles in the epicardium were all selected to quantify the immunoreactive areas. This elimination of oval fascicles (maximum diameter/minimum diameter ≥2) allowed us to avoid quantifying tangentially oriented axons. The selected fascicles were captured by a digital camera (D1, Nikon, Tokyo, Japan) connected to a microscope (BX-50, Olympus, Tokyo, Japan) with an objective ×40. The contour of the endoneurium was traced on a digitizer coupled with a liquid crystal display (PL-400, Wacom, Saitama, Japan). On the digitalized 8-bit RGB image of each endoneurium, the area of the entire endoneurium (fascicle area), TH+ area and NF+ area were measured using a standardized procedure on software (Adobe Photoshop 5.5 and NIH-image 1.62) as shown in Figure 1. Firstly, each digitalized image was transformed into an 8-bit gray scale (0:black-255:white) as follows. Several areas with the most intense immunoreactivity were selected and the mean value of these areas was calibrated to 50 on the 8-bit gray scale. In the same way, the mean value of several unstained areas was calibrated to 255. Based on these 2 calibration points, the entire image was transformed linearly into an 8-bit gray scale. This procedure enabled us to minimize the difference of brightness among the original digitalized images. Based on this transformed image, the average value (AV) and standard deviation value (SD) of stained axonal areas, which were arbitrarily selected, were calculated. The entire image was then binarized with the threshold defined as AV+SD. Areas with a pixel value below the threshold were judged to be immunoreactive areas. Finally the extracted areas were considered reasonable as immunoreactive areas compared with the original digitalized image.

Quantified values from several nerve fascicles from each subject were summed to yield the total fascicle area, total TH+ area and total NF+ area. The ratios of the total TH or NF+ area to the total fascicle area (TH/fascicle of NF/fascicle), the ratio of the total TH+ area to the total NF+ area (TH/NF) and the difference between the total TH+ areas and the total NF+ areas (NF-TH) were calculated for each subject. Differences in these calculated values between the PD and control groups were analyzed with the Mann-Whitney U test.

Triple immunofluorolabeling. Deparaffinized sections from a patient and a control subject were treated in a microwave oven with citrate buffer 3 times for 6 minutes, and then with 2% hydrogen peroxide for 30 minutes. Firstly, they were incubated with the anti-MBP antibody (diluted to 1:9000, which is detectable after catalyzed reporter deposition amplification) at 4°C for 2 days. They were incubated with anti-rabbit IgG made from goat conjugated to horseradish peroxidase (HRP, 1:1000; Pierce, Rockford, Ill). The HRP signal was amplified with biotinylated tyramide (1:1000; Perkin-Elmer, Boston, Mass) and then visualized with Cy-5 conjugated to streptavidin (1:200; Kirkegaard & Perry, Gaithersberg, Md). Subsequently, sections were incubated with a mixture of the anti-NF mouse monoclonal antibody (1:1000) and the anti-TH rabbit polyclonal antibody (1:100) at 4°C for another 2 days in the dark. These 2 antibodies were visualized with a mixture of anti-mouse IgG made from sheep conjugated with rhodamine (1:200, Jackson ImmunoResearch, West Grove, Pa) and anti-rabbit IgG made from goat conjugated with FITC (1:200, Vector), which could selectively visualize the anti-TH antibody because of insufficient sensitivity to the diluted anti-MBP antibody (20, 34).

RESULTS

H&E and immunohistochemical staining (Figure 2). H&E staining of the sections revealed several nerve fascicles, mostly transverse-sectional, in the epicardium. There was no apparent difference in the number and size of those nerve fascicles between the control and PD groups.

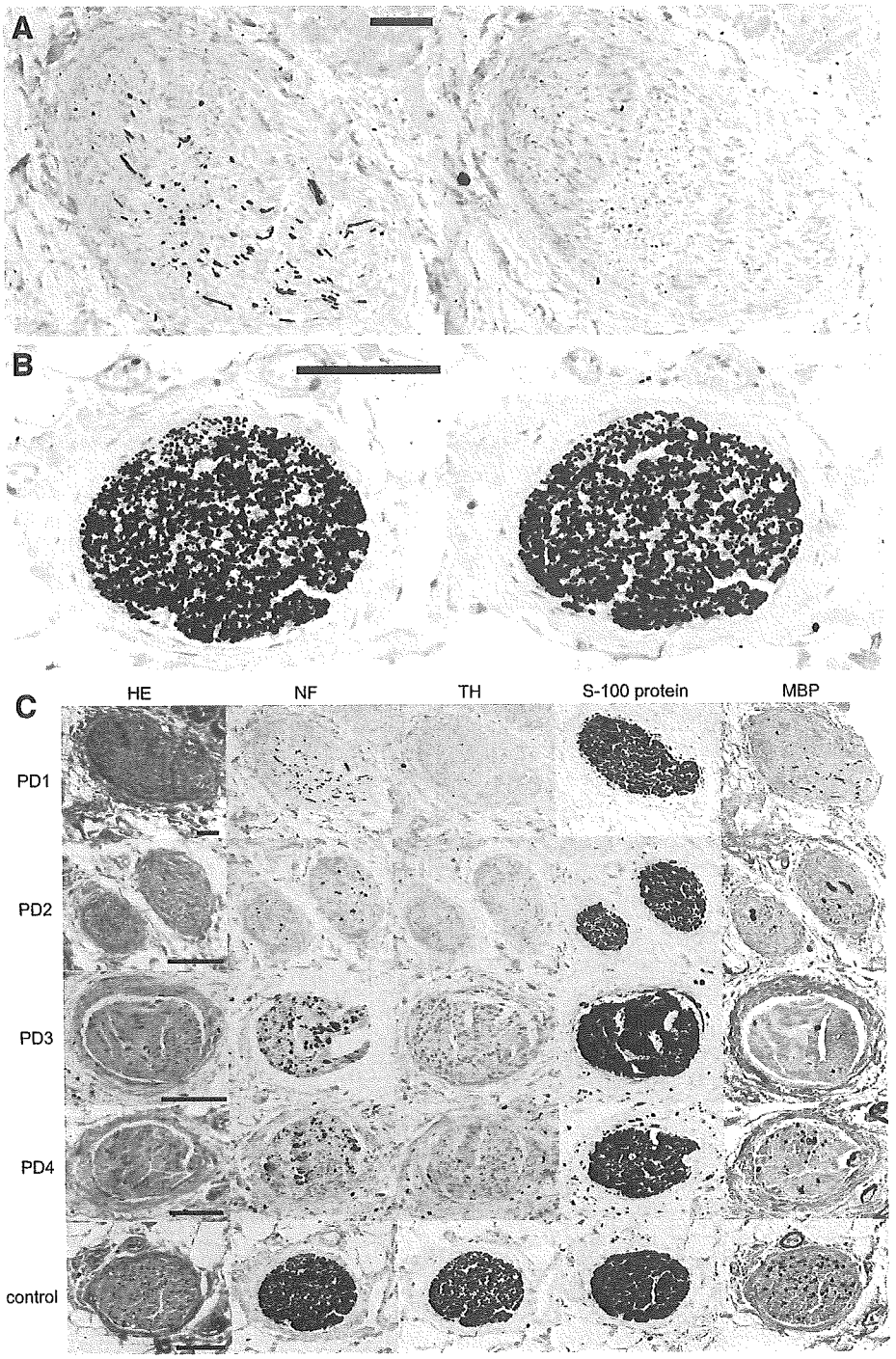

Figure 2. *H&E and immunohistochemical staining.* **A.** In the PD patient (PD 1), neurofilament (NF)-immunoreactive axons (Left) were sparse and tyrosine hydroxylase (TH)-immunoreactive axons (Right) were nearly absent. **B.** The control subject (control 4) showed numerous NF-immunoreactive axons (Left) and TH-immunoreactive axons (Right). **C.** Representative nerve fascicle in each patient or control subject (control 4) were shown. In all patients, NF-immunoreactive axons and TH-immunoreactive axons drastically decreased in number whereas S-100 protein-immunoreactive structures were equally preserved. A few myelin basic protein (MBP)-immunoreactive structures were seen in the fascicles of the epicardium and the number was smaller in patients than in control subjects. Scale bar = 100 μm.

In the control subjects, numerous NF+ axons were shown in the fascicle. Many TH+ axons were also seen, although they were smaller in number than NF+ axons. S-100 protein+ structures were also numerous, whereas MBP+ structures were comparatively sparse.

In the PD patients, NF+ axons were sparse and TH+ axons were nearly absent. A few MBP+ structures were seen, but the

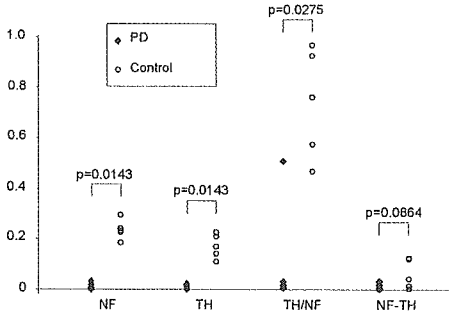

Figure 3. *Results of quantification for immunoreactive areas.* Mann-Whitney U tests were used for the statistical analysis between the patient (PD) and control group(Control).

number was smaller than in the control subjects. S-100 protein+ structures were numerous and equally preserved compared with those in the control subjects.

Quantitative analysis (Figure 3). In the control subjects, the ratios of TH/NF, which were in the range of 47% to 97%, revealed that most of the axons in the nerve fascicles in the epicardium were immunoreactive to TH. Both ratios of TH/fascicle and NF/fascicle obviously and significantly decreased in the PD group. The ratio of TH/NF also significantly decreased in the PD group. On the other hand, the difference of NF-TH showed a tendency to be smaller in the PD group, although it did not reach statistical significance.

Triple immunofluorolabeling (Figure 4). In the control subject (Figure 4B), numerous NF+ axons (red) were observed in nerve fascicles and most were immunoreactive to TH (green). MBP+ structures (blue) were sparse, and some surrounded TH+ axons as well as TH- axons. In the PD patient (Figure 4A), a fairly small number of NF+ axons and fewer MBP+ structures were recognized but TH+ axons were absent.

DISCUSSION

In the last few years, cardiac sympathetic dysfunction in PD has been revealed by the decreased cardiac uptake of sympathoneural tracers detected in SPECT or PET studies. We recently reported a marked decrease in TH+ axons in PD patients based on histological examination of the epicardium of the left ventricular anterior wall. Furthermore, in this case-control study, we expanded this observation by quantifying TH+ axons and NF+ axons in a series of patients with or without PD.

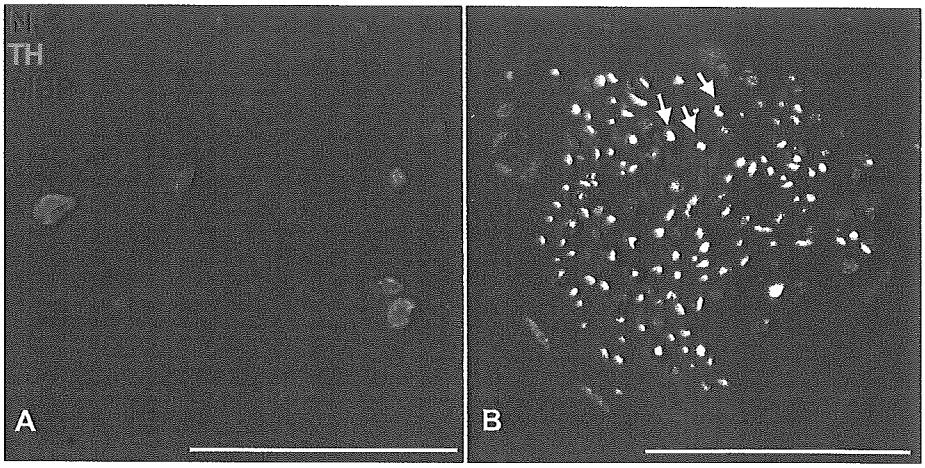

Figure 4. *The nerve fascicles in the epicardial spaces immunofluorolabeled with anti-NF (red), anti-TH (green) and anti-MBP (blue) antibodies.* **A.** PD patient. **B.** Control subject. In PD (**A**), TH-immunoreactive nerve fibers almost disappeared, and NF-immunoreactive nerve fibers and MBP-immunoreactive structure were markedly decreased. In the control subject (**B**), most NF-immunoreactive nerve fibers were also immunoreactive to TH (yellow), and, some were surrounded by MBP-immunoreactive structures (arrow in B). Scale bar = 50 μm.

Immunohistochemical staining revealed that the nerve fascicle in the epicardium contains a large number of TH+ axons in normal individuals. The high proportion of TH/NF in quantitative analysis indicated that TH+ axons occupy more than half of all axons in each fascicle. This TH+ dominant proportion is consistent with the previously reported ratio of catecholaminergic axons to cholinergic axons in the ventricular myocardium (2, 11). TH is a rate-limiting enzyme in catecholamine synthesis. The presence of TH in an axon is considered to indicate that the axon is catecholaminergic, and it has been used as a marker for locating presumptive sympathetic neural tissue (18). Recent studies demonstrated that TH could be also present in non-sympathetic tissue, such as the cranial parasympathetic ganglia of rat (9) or human cardiac ganglia (31), while its functional relevance in relation to the nature of the axons remains speculative. The existence of TH, therefore, is unable to prove conclusively by itself that the tissue is sympathetic. However, in the myocardium, noradrenalin is the dominant species among catecholamines (21, 28) and its tissue concentration is drastically reduced after stellectomy in rats (14, 27) and guinea pigs (7). This suggests that TH+ axons in the epicardium of the left ventricle presumably represent sympathetic axons, mainly noradrenergic axons originating from the cervico/thoracic sympathetic ganglia. The disappearance of TH+ axons in transplanted human hearts (30, 37) also indicates that TH+ axons are extrinsic, and is compatible with this interpretation.

The immunohistochemical staining for NF and TH showed a drastic decrease of NF+ axons and a more profound decrease of TH+ axons in PD. This finding indicated not merely the loss of the catecholamine synthesis enzyme, TH, but also the depletion of the sympathetic axons themselves. It means that the cardiac sympathetic nerves are morphologically degenerated. This offered new morphological evidence for the involvement of the cardiac sympathetic nerves in addition to the functional evidence that had been shown by PET or SPECT studies.

The near complete disappearance of TH+ axons and significant decrease in TH/NF in the PD group show that the sympathetic nerves were profoundly and preferentially involved in PD patients. On the other hand, NF-TH, that represents TH- axons, tended to be less frequent in PD, although the difference was not statistically significant. It is therefore possible that TH- axons are not involved. The PD related-depletion of TH- axons, if present, could have been overlooked because of the small number of TH- axons, leaving the possibility that the non-catecholaminergic axon is also involved in PD. Although the origin and nature of these non-catecholaminergic axons remain speculative, they may be from intrinsic neurons where Lewy bodies were previously found (10, 36).

According to PET or SPECT study, the extent of involvement in PD seems to vary

in the sympathetic nervous system. Decreased uptake of the tracers, 6F-DA or MIBG, was noted only in the heart, the thyroid gland and renal cortex, and the decrease in the heart was most prominent (5, 6, 29, 33). Moreover, there also seem to be differences among the parts of the heart. The PET study revealed that 6F-DA radioactivity was more severely decreased in the left ventricular free-wall than in the interventricular septum or the right myocardium (6, 12). Thus, the left ventricular anterior wall was expected to be one of the parts where the sympathetic nerve was most severely affected. We investigated this part of the heart pathologically and ascertained that the sympathetic nerves nearly disappeared.

There are several reports quantifying the TH protein content or TH activity in the central nervous system on postmortem examinations in PD. The TH protein content in PD decreased to 2.7% in the caudate nucleus, 5.3% in the putamen and 16% in substantia nigra compared with the control (17). TH activity decreased to 9.2% to 27.4% in the caudate nucleus, 4.1% to 21.6% in the putamen, 11.9% to 35.1% in the substantia nigra, 11.6% to 50.7% in the globus pallidus and 13% in the locus ceruleus (13, 16, 19). Our study revealed that in the epicardium of the left ventricular anterior wall, TH+ axons nearly completely disappeared in PD and the TH/fascicle ratio measured by quantitative analysis decreased to 1.1% of the control. Although there are differences in the measured object, it can be said that the cardiac sympathetic nerves in the left ventricular anterior wall are affected as much as the dopaminergic nerves in the central nervous system.

The sympathetic innervation to the ventricular working myocardium is thought to be mainly through the para-arterial route in the epicardium (15), consistent with the observation that the number of TH+ axons in the subepicardial area were larger than in the subendocardial area (11). The nerve fascicles in the epicardium, therefore, presumably contain sympathetic efferent axons innervating the working myocardium from the cervico/thoracic sympathetic ganglia. The depletion of TH+ axons in the epicardium represents the effacement of their distal axons and terminals, and therefore indicates cardiac sympathetic denervation in PD. The decreased cardiac uptake of these tracers is assumed to result from the effacement of these terminals since 6F-DA and MIBG are taken up by and stored in the adrenergic nerve terminals as with catecholamines (1, 38).

In addition, our study showed small number of myelinated axons in the epicardium, and the triple immunofluorolabeling unexpectedly demonstrated that some of the TH+ axons, although very small in number, were myelinated. The postganglionic sympathetic axons are generally considered unmyelinated C-fiber (35). Although the sympathetic afferent nerves consist of unmyelinated axons, it is uncertain and doubtful whether they are catecholaminergic. Neurotransmitters in the sympathetic afferent nerves are presumably considered substance P or neuropeptide K (26). As there was a report suggesting the existence of myelinated sympathetic postganglionic axons in a cat (3), our observation may indicate that the cardiac postganglionic sympathetic nerve contains tiny numbers of myelinated axons in humans.

In considering the pathogenesis of PD, the cardiac sympathetic nerves have not been emphasized as much as the central nervous system. This may be due to clinical absence of cardiac manifestations and the difficulty in detecting abnormalities. Because physiological functions of these sympathetic fibers in the myocardium are not well characterized, it is hard to predict the outcome after their depletion. Although diminished heart rate variability spectral measures of the variability have been reported in PD (8), routine electrocardiogram or ultrasound cardiography usually fail to demonstrate abnormalities. Indeed, all thirty-six PD patients in our previous study with decreased cardiac uptake of MIBG showed normal left ventricular function by ultrasound cardiography and most of them did not show serious arrhythmias and ST changes by 24-hour Holter electrocardiography (24). Among four PD patients in the present study, asymptomatic second degree A-V block of Mobitz type was the only abnormality in cardiac function. Because decreased cardiac uptake is not necessarily correlated with the presence of orthostatic hypotension nor with cardiac dysfunctions (5, 24), it is possible that near complete absence of sympathetic axons, first identified in the present study, is not related to clinically detectable manifestations. This is in agreement with the observation that left ventricular functions of transplanted heart under resting condition are quite normal even before sympathetic innervation is re-established (4). However, we should pay attention that decreased motor activity in PD patients may allow cardiac abnormalities, even if present, to remain unnoticed. Awareness of this sympathetic denervation, however, may raise attention to cardiac functions in PD patients and give clues to identify more subtle changes of cardiac functions so far not detectable but possibly linked to this sympathetic denervation.

This study demonstrated pathologically profound involvement in the cardiac sympathetic nervous system, which is catecholaminergic in common with the nigrostriatal nervous system. This may afford a new clue to elucidating the pathogenesis of PD.

REFERENCES

1. Chiueh CC, Zukowska-Grojec Z, Kirk KL, Kopin IJ (1983) 6-Fluorocatecholamines as false adrenergic neurotransmitters. *J Pharmacol Exp Ther* 225:529-533.

2. Chow LT, Chow WH, Lee JC, Chow SS, Anderson RH, Gosling JA (1998) Postmortem changes in the immunohistochemical demonstration of nerves in human ventricular myocardium. *J Anat* 192:73-80.

3. Emery DG, Foreman RD, Coggeshall RE (1978) Categories of axons in the inferior cardiac nerve of the cat. *J Comp Neurol* 177:301-310.

4. Frank MB, Peter U, Nina S, Stephan GN, Bruno R, Markus S (2001) Myocardial Efficacy and Sympathetic Reinnervation After Orthotopic Heart Transplantation. *Circulation* 103:1881-1886

5. Goldstein DS, Holmes CS, Dendi R, Bruce SR, Li ST (2002) Orthostatic hypotension from sympathetic denervation in Parkinson's disease. *Neurology* 58:1247-1255.

6. Goldstein DS, Holmes C, Li ST, Bruse S, Metman LV, Cannon RO (2000) Cardiac sympathetic denervation in Parkinson disease. *Ann Intern Med* 133:338-347.

7. Goto K, Longhurst PA, Cassis LA, Head RJ, Taylor DA, Rice PJ, Fleming WW (1985) Surgical sympathectomy of the heart in rodents and its effect on sensitivity to agonists. *J Pharmacol Exp Ther* 234:280-287.

8. Haapaniemi TH, Pursiainen V, Korpelainen JT, Huikuri HV, Sotaniemi KA, Myllyl VV (2001) Ambulatory ECG and analysis of heart rate variability in Parkinson's disease. *J Neurol Neurosurg Psychiatry* 70:305-310

9. Hardebo JE, Suzuki N, Ekblad E, Owman C (1992) Vasoactive intestinal polypeptide and acetylcholine coexist with neuropeptide Y, dopamine-beta-hydroxylase, tyrosine hydroxylase, substance P or calcitonin gene-related peptide in

neuronal subpopulations in cranial parasympathetic ganglia of rat. *Cell Tissue Res* 267:291-300.

10. Iwanaga K, Wakabayashi K, Yoshimoto M, Tomita I, Satoh H, Takashima H, Satoh A, Seto M, Tsujihata M, Takahashi H (1999) Lewy body-type degeneration in cardiac plexus in Parkinson's and incidental Lewy body diseases. *Neurology* 52:1269-1271.

11. Kawano H, Okada R, Yano K (2003) Histological study on the distribution of autonomic nerves in the human heart. *Heart Vessels* 18:32-39.

12. Li ST, Dendi R, Holmes C, Goldstein DS (2002) Progressive loss of cardiac sympathetic innervation in Parkinson's disease. *Ann Neurol* 52:220-223.

13. Lloyd KG, Davidson L, Hornykiewicz O (1975) The neurochemistry of Parkinson's disease: effect of L-dopa therapy. *J Pharmacol Exp Ther* 195:453-464.

14. Maccarrone C, Jarrott B (1987) Differential effects of surgical sympathectomy on rat heart concentrations of neuropeptide Y-immunoreactivity and noradrenaline. *J Auton Nerv Syst* 21:101-107.

15. Martins JB, Zipes DP (1980) Epicardial phenol interrupts refractory period responses to sympathetic but not vagal stimulation in canine left ventricular epicardium and endocardium. *Circ Res* 47:33-40.

16. McGeer PL, McGeer EG (1976) Enzymes associated with the metabolism of catecholamines, acetylcholine and gaba in human controls and patients with Parkinson's disease and Huntington's chorea. *J Neurochem* 26:65-76.

17. Mogi M, Harada M, Kiuchi K, Kojima K, Kondo T, Narabayashi H, Rausch D, Riederer P, Jellinger K, Nagatsu T (1988) Homospecific activity (activity per enzyme protein) of tyrosine hydroxylase increases in parkinsonian brain. *J Neural Transm* 72:77-82.

18. Molinoff PB, Axelrod J (1971) Biochemistry of catecholamines. *Annu Rev Biochem* 40:465-500.

19. Nagatsu T, Yamaguchi T, Rahman MK, Trocewicz J, Oka K, Hirata Y, Nagatsu I, Narabayashi H, Kondo T, Iizuka R (1984) Catecholamine-related enzymes and the biopterin cofactor in Parkinson's disease and related extrapyramidal diseases. *Adv Neurol* 40:467-473.

20. Nakamura A, Uchihara T (2004) Dual enhancement of triple immunofluorescence using two antibodies from the same species. *J Neurosci Methods* 135:67-70.

21. Neubauer B, Christensen NJ (1976) Norepinephrine, epinephrine, and dopamine contents of the cardiovascular system in long-term diabetics. *Diabetes* 25:6-10.

22. Orimo S, Oka T, Miura H, Tsuchiya K, Mori F, Wakabayashi K, Nagao T, Yokochi M (2002) Sympathetic cardiac denervation in Parkinson's disease and pure autonomic failure but not in multiple system atrophy. *J Neurol Neurosurg Psychiatry* 73:776-777.

23. Orimo S, Ozawa E, Nakade S, Hattori H, Tsuchiya K, Taki K, Takahashi A (2003) [^{123}I] metaiodobenzylguanidine myocardial scintigraphy differentiates corticobasal degeneration from Parkinson's disease. *Intern Med* 42:127-128.

24. Orimo S, Ozawa E, Nakade S, Sugimoto T, Mizusawa H (1999) ^{123}I-metaiodobenzylguanidine myocardial scintigraphy in Parkinson's disease. *J Neurol Neurosurg Psychiatry* 67:189-194.

25. Orimo S, Ozawa E, Oka T,Nakade S, Tsuchiya K, Yoshimoto M, Wakabayashi K, Takahashi H (2001) Different histopathology accounting for a decrease in myocardial MIBG uptake in PD and MSA. *Neurology* 57:1140-1141.

26. Owman C (1988) Autonomic innervation of the cardiovascular system. In: *Handbook of Chemical Neuroanatomy*, Bjorklund A, Hokfelt T (eds.), Volume 6, The Peripheral Nervous System, Chapter IX, pp.327-340, Elsevier: Amsterdam, New York, Oxford

27. Pardini BJ, Lund DD, Schmid PG (1990) Innervation patterns of the middle cervical--stellate ganglion complex in the rat. *Neurosci Lett* 117:300-306.

28. Petch MC, Nayler WG (1979) Concentration of catecholamines in human cardiac muscle. *Br Heart J* 41:340-344

29. Reinhardt MJ, Jungling FD, Krause TM, Braune S (2000) Scintigraphic differentiation between two forms of primary dysautonomia early after onset of autonomic dysfunction: value of cardiac and pulmonary iodine-123 MIBG uptake. *Eur J Nucl Med* 27:595-600.

30. Schuurman HJ, Plomp S, Wijngaard PL, Slootweg PJ, de Jonge N (1993) Innervation of the endomyocardium in the first period after heart transplantation. *Transplantation* 56:85-88.

31. Singh S, Johnson PI, Javed A, Gray TS, Lonchyna VA, Wurster RD (1999) Monoamine- and histamine-synthesizing enzymes and neurotransmitters within neurons of adult human cardiac ganglia. *Circulation* 99:411-419.

32. Takahashi A (1991) Autonomic nervous system disorders in Parkinson's disease. *Eur Neurol* 31(Suppl 1):41-47.

33. Taki J, Nakajima K, Hwang EH, Matsunari I, Komai K, Yoshita M, Sakajiri K, Tonami N (2000) Peripheral sympathetic dysfunction in patients with Parkinson's disease without autonomic failure is heart selective and disease specific. *Eur J Nucl Med* 27:566-573.

34. Uchihara T, Nakamura A, Nakayama H, Arima K, Ishizuka N, Mori H, Mizushima S (2003) Triple immunofluorolabeling with two rabbit polyclonal antibodies and a mouse monoclonal antibody allowing three-dimensional analysis of cotton wool plaques in Alzheimer disease. *J Histochem Cytochem* 51:1201-1206.

35. Van Stee EW (1978) Autonomic innervation of the heart. *Environ Health Perspect* 26:151-158.

36. Wakabayashi K, Takahashi H (1997) Neuropathology of autonomic nervous system in Parkinson's disease. *Eur Neurol* 38 Suppl 2:2-7.

37. Wharton J, Polak JM, Gordon L, Banner NR, Springall DR, Rose M, Khagani A, Wallwork J, Yacoub MH (1990) Immunohistochemical demonstration of human cardiac innervation before and after transplantation. *Circ Res* 66:900-912.

38. Wieland DM, Brown LE, Tobes MC, Rogers WL, Marsh DD, Mangner TJ, Swanson DP, Beierwaltes WH (1981) Imaging the primate adrenal medulla with [^{123}I] and [^{131}I] meta-iodobenzylguanidine: concise communication. *J Nucl Med* 22:358-364.

39. Yoshita M (1998) Differentiation of idiopathic Parkinson's disease from striatonigral degeneration and progressive supranuclear palsy using iodine-123-meta iodobenzylguanidine myocardial scintigraphy. *J Neurol Sci* 155:60-67.